FRACTURE ANALYSIS OF SEMI-ELLIPTICAL SURFACE CRACKS IN DUCTILE MATERIALS

FINAL REPORT
NASA MARSHALL SPACE FLIGHT CENTER GRANT NAG8-1883

S.R. Daniewicz
Professor, Department of Mechanical Engineering
Mississippi State University
662-325-7322
daniewicz@me.msstate.edu

J.C. Newman, Jr.
Professor, Department of Aerospace Engineering
Mississippi State University
662-325-1521
j.c.newman.jr@ae.msstate.edu

A.M. Leach
Graduate Research Associate
Department of Mechanical Engineering
Mississippi State University

submitted to:
NASA Technical Officer: W. Gregg
NASA Grant Administrator: L.P. Southgate

8/25/04

TABLE OF CONTENTS

CHAPTER

APPENDIX

LIST OF TABLES

LIST OF FIGURES

CHAPTER I

INTRODUCTION AND LITERATURE REVIEW

I.A Overview

Accurate life assessment of structural components may require advanced life prediction criteria and methodologies. Structural components often exhibit several different types of defects, among the most prevalent being surface cracks.

A semi-elliptical surface crack subjected to monotonic loading will exhibit stable crack growth until the crack has reached a critical size, at which the crack loses stability and fracture ensues (Newman, 2000). The shape and geometry of the flaw are among the most influential factors. When considering simpler crack configurations, such as a through-the-thickness crack, a three-dimensional (3D) geometry may be modeled under the approximation of two-dimensional (2D) plane stress or plane strain. The more complex surface crack is typically modeled numerically with the Finite Element Method (FEM). A semi-elliptical surface crack is illustrated in Figure 1-1.

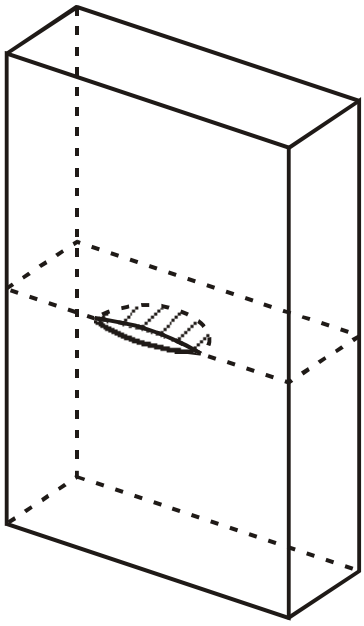

Figure 1-1 Surface Crack in a Plate

Characterizing surface crack growth and fracture under monotonic loading requires knowledge of the material behavior and stress state surrounding the crack front. In cases where the plastic zone surrounding the crack tip is of small magnitude relative to the distance to the nearest boundary, Linear Elastic Fracture Mechanics (LEFM) may be applied for a simple determination of failure loads and related quantities. High levels of plasticity may necessitate use of Elastic-Plastic Fracture Mechanics (EPFM).

A mathematical description of the conditions required to induce crack growth in an elastic body was first presented by Griffith (Griffith, 1920) in the form of an energy balance equation. Crack-tip stress field expansions for an elastic body were later derived by Irwin (Irwin, 1956) and Williams (Williams, 1957). The crack-tip stress field expansion is dominated by a constant within the first term, the stress intensity factor

(SIF) *K* as denoted by Irwin. Similarly, the path independent *J*-integral was proposed by Rice (Rice, 1968) as the dominant parameter in the elastic-plastic stress field expansion. Dodds et al (Dodds, 1993) remark that two fundamental concepts underlie both LEFM and EPFM:

1) the relevant crack-tip singularity dominates over microstructurally significant size scales
2) the parameter *K* or *J* uniquely scales the amplitude of the near tip field.

I.B Finite Element Analysis

I.B.1 Overview

The embedded elliptical crack in an elastic body was first studied by Irwin (Irwin, 1962). Irwin provided the foundation for semi-elliptical surface crack Finite Element Analysis (FEA) investigations conducted by Ayres (Ayres, 1970) and Levy *et al*. (Levy, 1971), who used 3D elastic-plastic small strain formulations to obtain the plastic-zone shape and stress distribution around the crack front. McMeeking and Parks (McMeeking, 1979) and Shih and German (Shih, 1981) later utilized FEA to examine components under applied monotonic tension and bending in order to characterize the evolving stress fields near the crack-tip. A useful summary of the advances in the characterization of elastic-plastic crack-tip fields is presented by Parks (Parks, 1992)

Raju and Newman (Raju, 1979) (Newman, 1981) performed 3D elastic analyses to obtain *K* for semi-elliptical surface cracks for a range of crack sizes and loading types. The Raju-Newman *K* solutions have since been expanded by Fawaz and Andersson (Fawaz, 2004) who analyzed the corner crack at a hole configuration. The solutions were

extended to larger ranges of crack-depth-to-thickness and crack-depth-to-width ratios by utilizing higher levels of mesh refinement and large-scale computational resources not available to Raju and Newman. Trantina *et al.* (Trantina, 1983) also performed elastic-plastic surface crack FEA to establish the limitations of LEFM and to compute the *J*-integral for small cracks. Parks and Wang (Parks, 1992) presented *J*-integral values for surface cracks determined using detailed finite element solutions, and studied the effects of local crack front constraint on the fracture process.

I.B.2 Finite Element Mesh Design

One of the difficulties in applying FEA to surface cracked geometries lies in the generation of meshes suitable for accurate calculations in the crack-front region. The near tip stress fields in a cracked body are dominated by stress and strain gradients normal to the crack front due to the immobility of the material in front of the advancing crack. For reliable finite element calculations, the geometry must be adequately discretized in the region local to the crack front to capture these gradients. Faleskog (Royal Institute of Technology, Stockholm, Sweden) developed a code to generate semi-elliptical surface crack meshes based on a right-hand curvilinear elliptic coordinate system derived by Timoshenko (Timoshenko, 1970). Historically, meshes generated with the Faleskog code have produced reliable results (Faleskog, 1995) (Gao, 1998) (Aveline, 1999). However, it is difficult to generate a mesh without high aspect ratio elements. More recently, Structural Reliability Technologies of Boulder, CO (www.srt-boulder.com) have developed a commercial software package FEA-Crack capable of

generating meshes for various cracked geometries, including surface cracks. The FEA-Crack surface crack mesh is based on a rectangular coordinate system, and utilizes a highly discretized tube of elements around the crack front. The mesh is generated using a proprietary code; a license must be purchased in order to use the software. A typical FEA-Crack surface mesh is presented in Figure 1-2. Meshes generated with FEA-Crack were used for all analyses reported herein.

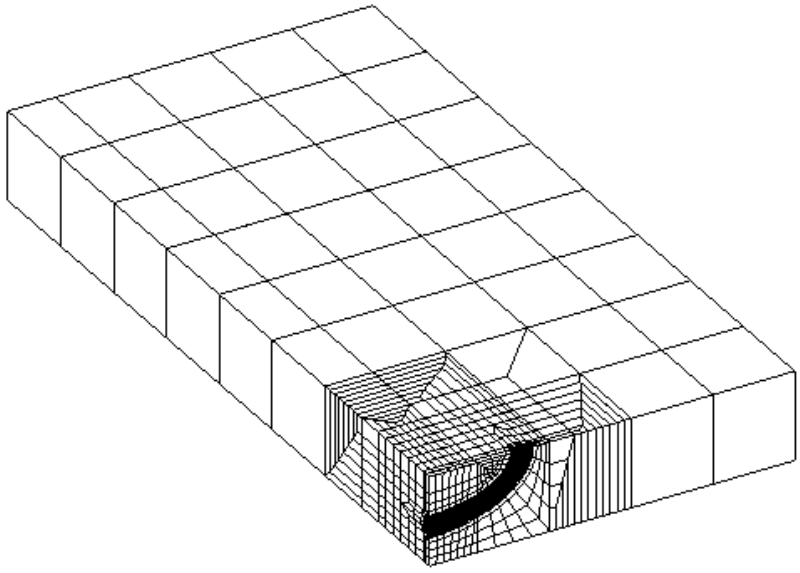

Figure 1-2.a Typical Semi-Elliptical Surface Crack Finite Element Mesh

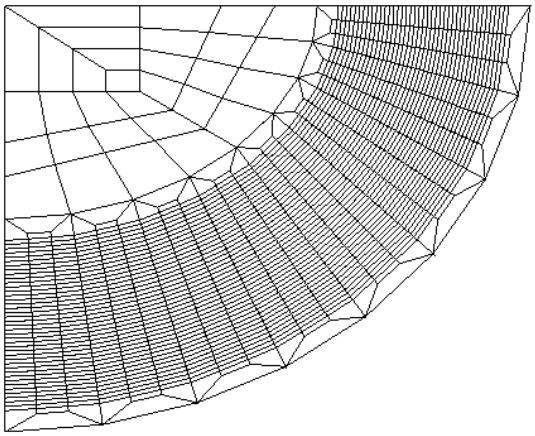

Figure 1-2.b Finite Element Mesh Details around the Crack Front

I.C Fracture Prediction Methodologies

The development of fracture prediction methodologies has been the topic of much research. The most accurate approach to predict structural integrity is to forecast the fracture process including initiation of crack growth, the extent of stable growth, and failure. Typically, fracture analyses are conducted by calculating a well-defined fracture mechanics parameter and comparing it to a critical value that has been determined through material testing. Hult and McClintock (Hult, 1956) discovered that under conditions of limited crack-tip plastic deformation, the details of the local elastic-plastic fields could be uniquely related to a single macroscopic parameter, such as *K* or *J,* scaling the intensity of crack-tip deformation. Parks (Parks, 1992) comments, "… that local crack tip fields can be characterized by a single parameter, and further, that fracture processes are driven by these fields, there exists a mechanistic rationale for constructing 'single parameter' fracture mechanics correlations of crack extensions."

I.C.1 Single Parameter Fracture Criteria

The amount of local yielding around the crack front dictates the appropriate parameter choice. In cases where the relative plastic zone size is small, as in brittle materials, *K* is the fracture controlling parameter. However, a larger plastic zone size indicates behavior typical of ductile materials, in which case the *J*-integral has been proven as a suitable parameter.

The SIF has been correlated to the energy release rate in a cracked body. It has been widely used to predict crack extension by characterizing failure as the point where *K* is equal to the plane strain fracture toughness, K_{IC}. Reuter *et al* (Reuter, 2002), compared the plane strain fracture toughness K_{IC} and K_{pk} (the peak *K* value around the perimeter of a part-through crack) for different materials loaded in tension and bending. Using the conventional criterion for monotonic loading to failure, ratios of K_{pk} / K_{IC} were found to be greater than 1.0 and in some cases were greater than 2.0, implying that conventional practices were conservative.

The *J*-integral has been used to correlate the initiation of crack growth in plastically deforming solids. When high levels of plastic deformation are present, the relationship between the *J*-integral and the crack-tip stress field lose a direct correlation (McMeeking, 1979) (Shih, 1981). The loss of *J*-dominance signifies a loss of constraint in the body and lends support for the incorporation of a second parameter in the fracture criterion.

I.C.2 Two Parameter Fracture Criteria

In an effort to more accurately predict failure under monotonic loading conditions, incorporation of a constraint term as a second parameter in fracture prediction criteria has been proposed by several investigators, including Hancock *et al*. (Hancock, 1991) (Hancock, 1993). Constraint refers to the buildup of stresses around a crack front due to restraint against in-plane and out-of-plane deformation. Newman *et al*. (Newman, 1995) present a precise description of constraint:

> Strain gradients that develop around a crack front cause the deformation in the local region to be constrained by the surrounding material. This constraint produces multi-axial stress states that complicate stress analyses and influence fatigue crack growth and fracture behavior. The level of constraint depends upon the crack configuration and crack location relative to external boundaries, the material thickness, the type and magnitude of loading, and the material stress strain properties.

Constraint has often been used within fracture mechanics in a qualitative manner, such as plane-stress or plane-strain constraint. However, efforts to quantify the influence of constraint on fracture have been the subject of much recent work. In order to use constraint in fracture prediction, the crack front stress state must be resolved with a numerical parameter defining the level of constraint along the crack front. McMeeking and Parks (McMeeking, 1979) expressed the plastic stress concentration factor $K_{\sigma p}$ as a measure of constraint

$$K_{\sigma p} = \max_x \left(\frac{\sigma_{yy}}{R_{eL}} \right) \tag{1-1}$$

where σ_{yy} is the normal (crack opening) stress, R_{eL} is the lower yield point, and max_x is the maximum quantity in the x-direction. Several researchers (Rice, 1969) (Hancock, 1976) (McClintock, 1979) used a more general definition of constraint given by σ_m / σ_{vm},

where σ_m and σ_{vm} are the mean and equivalent stresses in the neighborhood of the crack-tip, respectively. Sommer and Aurich (Sommer, 1991) analyzed the mean-stress-to-equivalent-stress ratio for surface cracked specimens and showed how constraint (as defined in this manner) affected stable crack-growth behavior under monotonic loading conditions. Hancock *et al.* (Hancock, 1991) proposed the use of *T* stress, the stress that is in-plane and parallel to the crack surfaces, while others such as O'Dowd and Shih (O'Dowd, 1991) used the *Q* stress as a measure of stress triaxiality around the crack front. Newman *et al.* (Newman, 1993) proposed using the normal stress in the near-tip stress field as a measure of constraint. This measure of constraint was referred to as the global constraint factor α_g, the average normal stress acting over the plastic region through the thickness of a through crack. The hyper-local constraint factor α_h, developed by Aveline and Daniewicz (Aveline 1999), is defined as the average of the normal-stress-to-flow-stress ratio along a line emanating from the crack front to the plastic zone boundary along the crack plane. Newman *et al.* (Newman, 1999) and Reuter *et al.* (Reuter, 2002) used α_h to predict initiation and fracture of surface cracks in brittle materials under tension and bending loads and correlated these results with cracked through-the-thickness bend specimens. Fracture initiation was predicted to occur at the load corresponding to the maximum $\alpha_h K$ value along the surface crack front. The approach predicted initiation load within ±20%, displaying the viability of α_h as a fracture criteria constraint parameter. Aveline and Daniewicz (Aveline, 1999) developed α_h for a range of crack sizes and loading types for brittle materials, but the approach has not yet been applied to ductile materials.

The objective herein is to extend the above work for application to a ductile material. *J*-integral and constraint factor distributions for a range of surface crack sizes and loading conditions were obtained. The fracture initiation location is then predicted to occur at the point of highest $J\alpha_h$. Finite element analyses were conducted on a wide range of surface crack configurations, and the *J*-integral and α_h values were calculated for each model. To verify the validity of the developed fracture prediction model, the Idaho National Engineering and Environmental Laboratories (INEEL) tested a large number of surface crack specimens, each loaded monotonically to failure. These specimens and particular surface crack configurations were modeled with the FEM. The analytical and experimental data is presented and the potential of $J\alpha_h$ as a fracture criterion is discussed.

CHAPTER II

NOMENCLATURE AND CONSTRAINT DEFINITION

II.A Crack Geometry and Loading

Cracked bodies are characterized by geometrical parameters describing the size and shape of the flaw. In the case of the surface crack, as shown in Figure 1-1, the notation is as follows and is presented in Figure 2-1: crack depth *a,* crack half-length *c,* specimen half-width *w,* specimen half-height *h,* and specimen thickness *t.* When discussing surface cracks, it is common to describe the size of the crack in terms of geometrical ratios relating the crack to the containing body, where the crack-depth-to-specimen-thickness ratio is *a/t* and the crack aspect ratio is *a/c*. Parameters that describe behavior along the surface-crack front require an angular measure defining the location of a point on the crack front; the preferred nomenclature is the parametric angle ϕ.

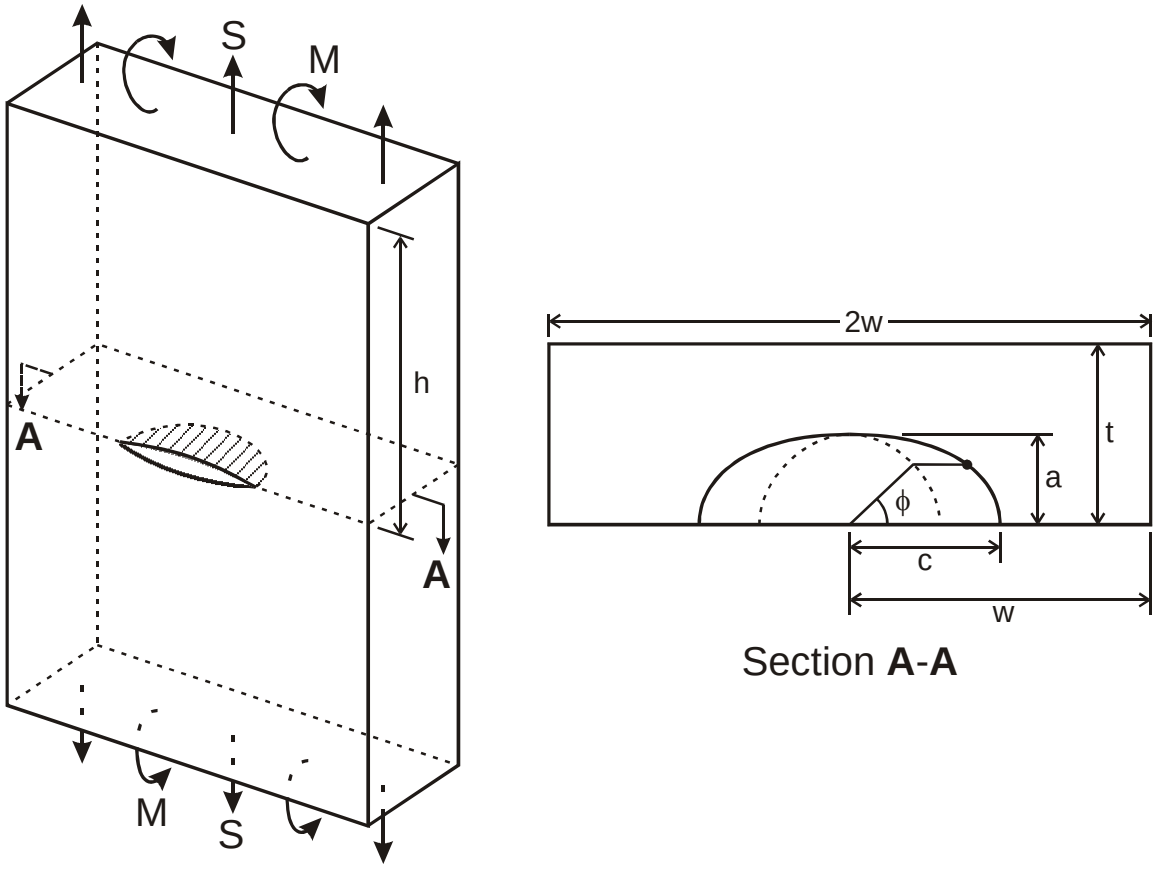

Figure 2-1 Surface Crack Configuration

Considering a point on the crack front, (x_i, y_i), the parametric angle may be calculated using Eq. 2.1. The free surface of the crack is defined as the location where $\phi = 0$, and the deepest point of penetration where $\phi = \pi/2$.

$$\phi = \sin^{-1}\left(\frac{y_i}{a}\right) \qquad (2\text{-}1)$$

The surface cracks modeled in this investigation have been subjected either to an applied monotonic tensile load S corresponding to a tensile stress σ_T or to a uniform bending moment M with a corresponding maximum bending stress of magnitude σ_B.

Surface cracked plates exhibit two planes of symmetry, one along the length (*y*-*z* plane), and the other along the width (*x*-*y* plane). The planes of symmetry and coordinate system orientation are presented in Figure 2-2.

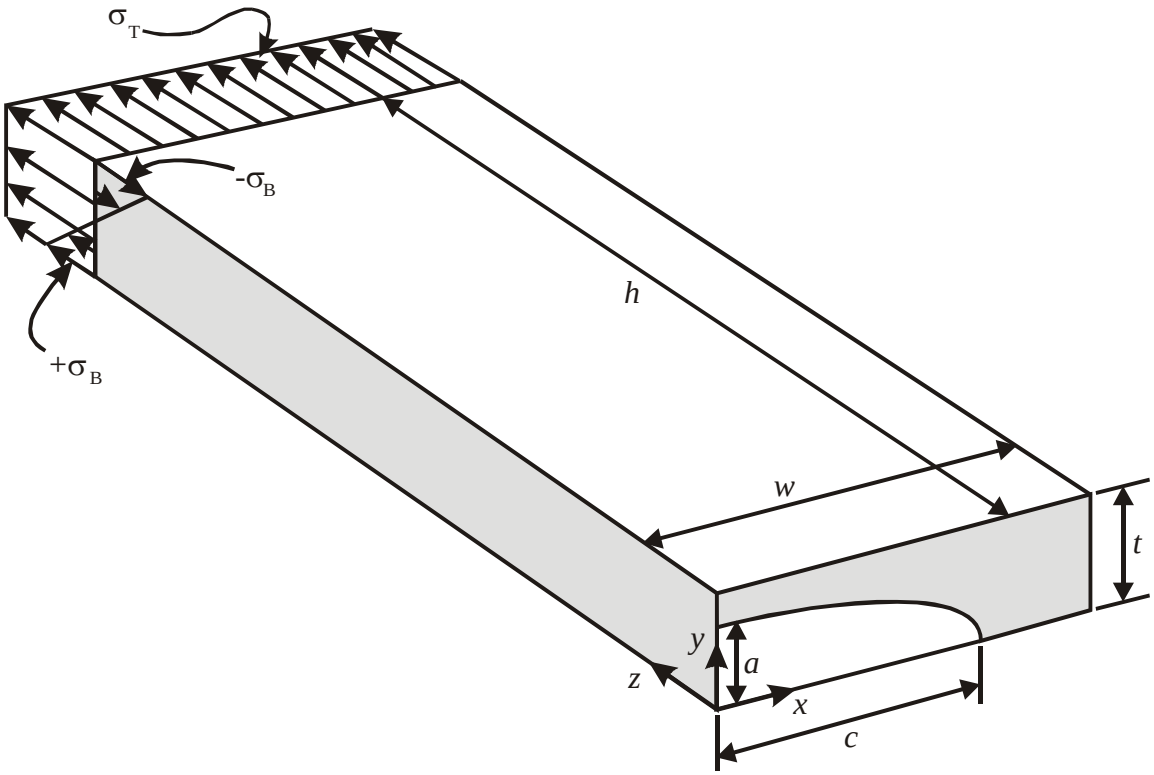

Figure 2-2 General Finite Element Model and Applied Loading

The presence of geometrical symmetry greatly reduces the modeling requirements and eases the computational burden. Also evident in Figure 2-2 is the crack plane, the *x*-*y* plane. The crack plane is the location of most concern for the analyses presented. The shaded region on the crack plane will be referred to as the uncracked ligament or the

material ahead of the crack front, while the white region on the crack plane will be denoted as the cracked ligament or the material behind the crack front.

II.B Constraint Definition

The definition of constraint considered is an extension of the global constraint factor α_g presented by Newman *et al*. (Newman, 1993). When a cracked body is subjected to an applied load, a small region of material directly ahead of the crack front will be elevated to a stress level beyond the material yield strength σ_o due to the immobility of the material ahead of the crack. Considering the von-Mises yield criterion, the material is said to have yielded when the equivalent stress or von-Mises stress σ_{vm} has reached σ_o. The von Mises stress is determined by the overall 3D stress state present in the body, see Eq. 2-2.

$$\sigma_{vm} = \sqrt{\frac{{\sigma_{xx}}^2 + {\sigma_{yy}}^2 + \left(\sigma_{xx} - \sigma_{yy}\right)^2 + 6{\tau_{xy}}^2}{2}} \tag{2-2}$$

Consider the simple 2D plane stress case of a notched body subjected to a tensile load, Figure 2-3. At an infinitesimal point *A* at the notch tip, the stress in the *x*-direction σ_x must be zero to satisfy the free-surface boundary condition. For the point *A* to be yielded, the stress in the *y*-direction σ_y must be equal to σ_o. Moving a small distance ahead of the notch tip to point B, the free surface boundary condition is no longer present, thus σ_x is no longer forced to a value of zero, and σ_y may be elevated above σ_o by a factor α. This factor defines the level of local normal stress constraint present in the plastic zone of the material.

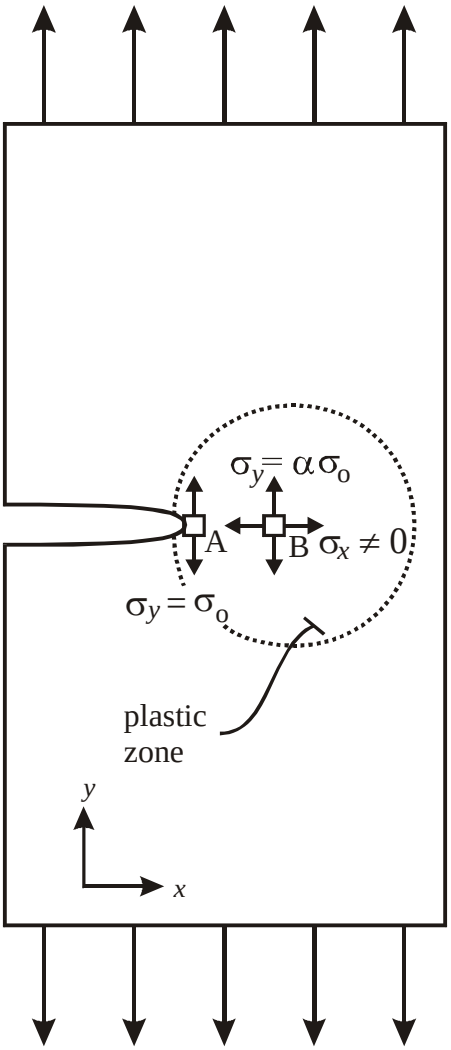

Figure 2-3 Two-Dimensional Constraint Definition

In three-dimensional stress space, the local constraint is magnified by the presence of stress triaxiality and the resistance to in-plane and out-of-plane deformation. The higher the constraint level the more plastic deformation near the notch will be restrained.

CHAPTER III

LABORATORY TESTING OF SURFACE CRACKS

III.A Test Plan

INEEL was contracted to perform mechanical testing on plates containing surface cracks by NASA and the FAA. A plan was presented to INEEL outlining the material selection, surface crack fabrication specifications, and testing guidelines. The material selected for testing was D6AC steel, heat-treated to a ductile condition. The heat treatment as dictated by the ATK-Thiokol standard was:

1. Austenitize under controlled atmosphere at 1615^{o}F+/-25^{o}F for 2.5 hours minimum.
2. Quench in molten salt bath at 325^{o}F maximum initial temperature, 15 minutes minimum.
3. Air cool to 175^{o}F
4. Snap temper in molten salt for 3 hours minimum at 310^{o}F to 345^{o}F
5. Clean metal to remove all salt
6. Temper to meet mechanical property requirements. Minimum of two temper cycles shall be used. Tempering temperature is 1070^{o}F - 1115^{o}F for 6 to 7 hours. Cool components in air to 175^{o}F max between tempering cycles.

After heat treatment, the material must satisfy the following property requirements:

1. Ultimate Tensile Stress: 200 ksi min - 225 ksi max
2. Yield Stress: 180 ksi min
3. Percent Elongation: 8% min
4. Reduction in Area: 25% min
5. K_{IC}: 90 ksi$\sqrt{in}$

The D6AC steel used for specimen fabrication satisfied the above requirements.

Twelve different surface crack shapes and sizes were identified as the crack configurations to be tested. The same configurations were to be tested monotonically under either remote tension or bending loads. The crack configurations are presented in Table 3-1:

Table 3-1 Proposed Surface Crack Configurations

BENDING LOADS				TENSILE LOADS			
a/c	*a/t*			*a/c*	*a/t*		
0.90	0.20	0.50	0.75	0.90	0.20	050	0.75
0.72	0.20	0.50	0.75	0.72	0.20	0.50	0.75
0.48	0.20	*	0.75	0.48	*	0.50	0.75
0.10	0.20	0.50	0.75	0.10	0.20	*	0.75

The crack sizes denoted by * show a negligible change in K_I around the perimeter of the surface crack as calculated by the Raju-Newman equations, thus were not proposed for inclusion in the test plan. The specimens were fabricated and a triangular starter notch was electrical-discharge machined (EDM) in the center of the specimen to aid crack initiation. All specimens, regardless of load type were pre-cracked under remote cyclic bending loads of unknown magnitude[1] to reach the desired initial crack size specification. Obtaining a specific crack size is a difficult procedure, thus the initial surface crack sizes were not identical to the proposed configurations. After pre-cracking, 14 tension and 8 bending specimens were available for testing. The specimens were loaded monotonically until a 5% potential drop was recorded, indicating that a small amount of crack extension had occurred. The load at the 5% potential drop was recorded. After the first occurrence

[1] Pre-cracking for the initial crack formation was not performed at INEEL and the load levels were not recorded. Shear lip formation was not observed on the fracture surfaces, indicating the pre-cracking levels were likely within reason.

of crack extension, the specimens were cyclically loaded at a reduced load level to mark the location and extent of stable crack growth. The specimens were subjected to three instances of crack extension and cyclic marking before loading to complete failure; however, only the first instance is considered in this study. The specimen and crack dimensions as well as maximum applied stress at the onset of first crack extension are presented in Table 3-2.a (tension) and Table 3-2.b (bending) below.

Table 3-2.aTension Specimen Specifications

Specimen ID	*a* (mm)	*c* (mm)	*t* (mm)	*w* (mm)	σ_T (MPa)
AT-01	1.22	1.6	6.26	25.28	1300.8
AT-02	1.46	1.76	6.32	25.46	1294.2
AT-04	3.20	4.44	6.35	25.40	1152.3
AT-05	3.33	4.75	6.35	25.40	1111.7
AT-06	3.27	4.56	6.34	25.50	1140.1
AT-07	4.13	6.78	6.40	25.39	1006.3
AT-08	4.27	6.97	6.33	25.36	992.5
AT-09	4.16	6.63	6.24	25.49	987.8
BT-01	4.61	9.80	6.35	25.40	841.0
BT-04	5.89	23.31	6.35	25.40	271.4
CT-01	3.49	6.44	6.22	25.44	872.5
CT-02	3.51	6.65	6.20	25.37	998.4
CT-03	3.38	6.56	6.29	25.31	1044.2
DT-02	1.73	6.42	6.35	25.40	1205.6

Table 3-2.b Bending Specimen Specifications

Specimen ID	*a* (mm)	*c* (mm)	*t* (mm)	*w* (mm)	σ_B (MPa)
AB-01	4.356	7.076	6.37	25.375	1720.6
AB-04	3.185	4.543	6.38	25.375	1574.5
AB-07	1.516	1.822	6.37	25.350	1969.6
BB-01	4.620	9.860	6.35	25.385	1369.8
BB-04	5.495	23.460	6.32	25.375	448.3
CB-01	1.712	2.690	6.36	25.37	2010.3
DB-03	2.314	6.487	6.36	25.35	1772.2
DB-04	3.880	15.850	6.34	25.385	1047.7

After loading each specimen to failure, a high-resolution digital image was taken of the fracture surfaces to show surface crack pre-cracking shape and size and the amount of crack extension. An image showing the details of the fracture surface is given in Figure 3-1. Sample tension and bending fracture surfaces are provided in Figures 3-2.a and 3-2.b, respectively.

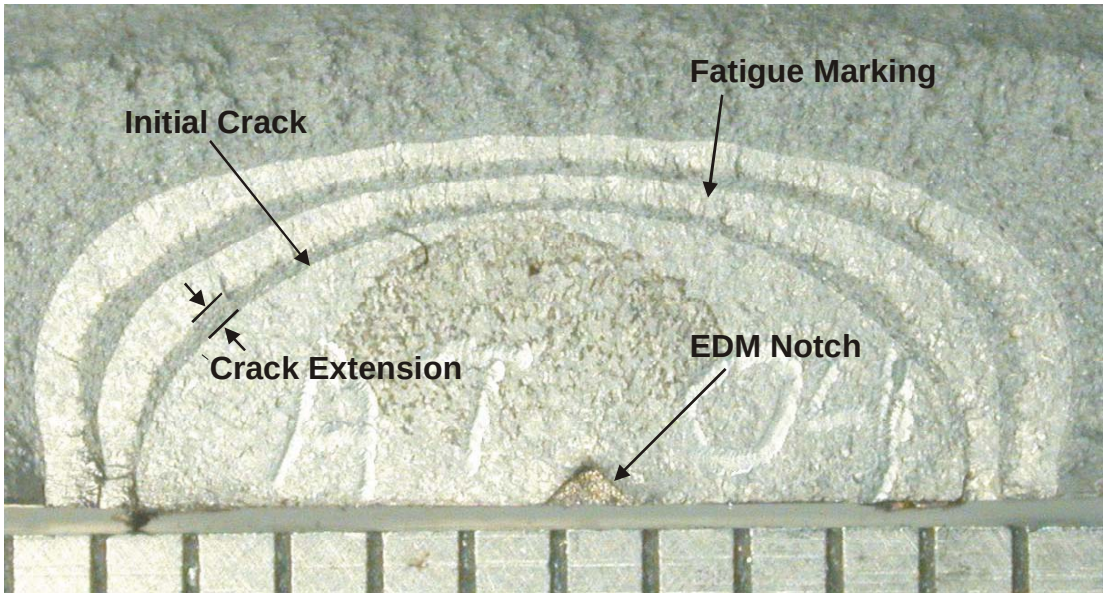

Figure 3-1 Surface Crack Fracture Surface Details

Figure 3-2.a Typical Surface Crack Fracture Surface (Tension)

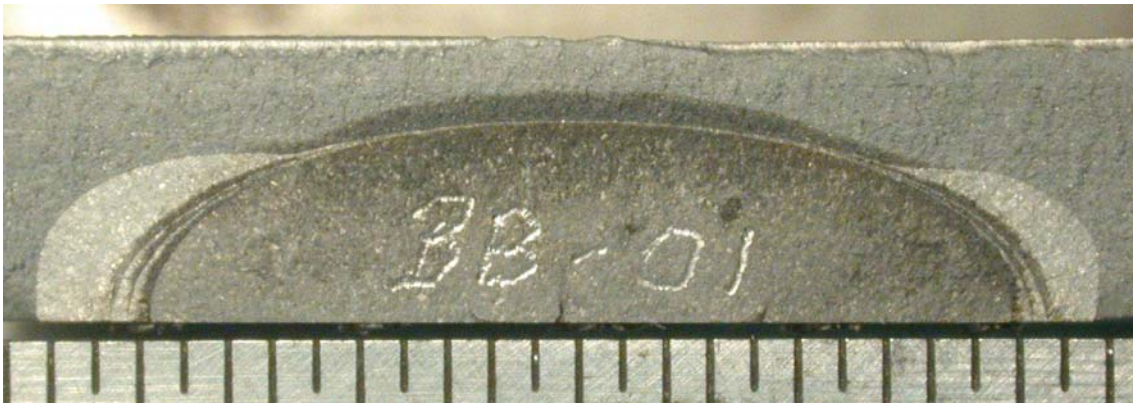

Figure 3-2.b Typical Surface Crack Fracture Surface (Bending)

In addition to the surface crack specimens tested, single-edge-bend (SEB) specimens were fabricated and tested to provide plots of J versus crack extension Δa. While not considered as part of this research, they may prove beneficial for future research.

CHAPTER IV

FINITE ELEMENT ANALYSIS OVERVIEW

WARP3D release 15 (WARP3D, 2004) was used in analyzing the 22 surface crack models (14 tension, 8 bending). FEA-Crack *version* 2.5.625 was employed to generate the surface crack meshes and the WARP3D input files. A preliminary verification for *J*-integral calculations was performed to ensure that the WARP3D solution parameters were being used correctly and that the surface crack meshes were adequately refined. The material model, mesh characteristics, and solution parameters are presented.

IV.A Preliminary Verification

J-integral calculations were verified against those published by Parks (Parks, 1992). Parks performed 3D elastic-plastic FEA on surface cracked plates under varying tensile and bending loads and calculated the *J*-integral as a function of ϕ around the crack front for each load level. To verify the calculation of *J* using WARP3D, finite element models were constructed of identical crack size, material model, and applied load level to those of Parks. The *J* solutions obtained from WARP3D were plotted against the Parks solutions for both the tension and bending cases. The *J* values were normalized by $(\varepsilon_o \sigma_o t \Sigma^2)$, where ε_o and σ_o are the yield strain and yield stress, respectively, *t* is the

thickness, and Σ is a loading parameter given by the applied stress divided by the yield stress. The comparisons are shown in Figures 4-1.a and 4-1.b. While the *J* solutions compare within reason, differences remain evident. The lack of agreement is likely due to a combination of mesh refinement limitations within the Parks solution and different methods of calculating the *J*-integral (Parks used the Virtual Crack Extension method whereas WARP3D uses the Domain Integral method). In view of these differences in analyses, WARP3D was considered a reliable means of calculating the *J*-integral.

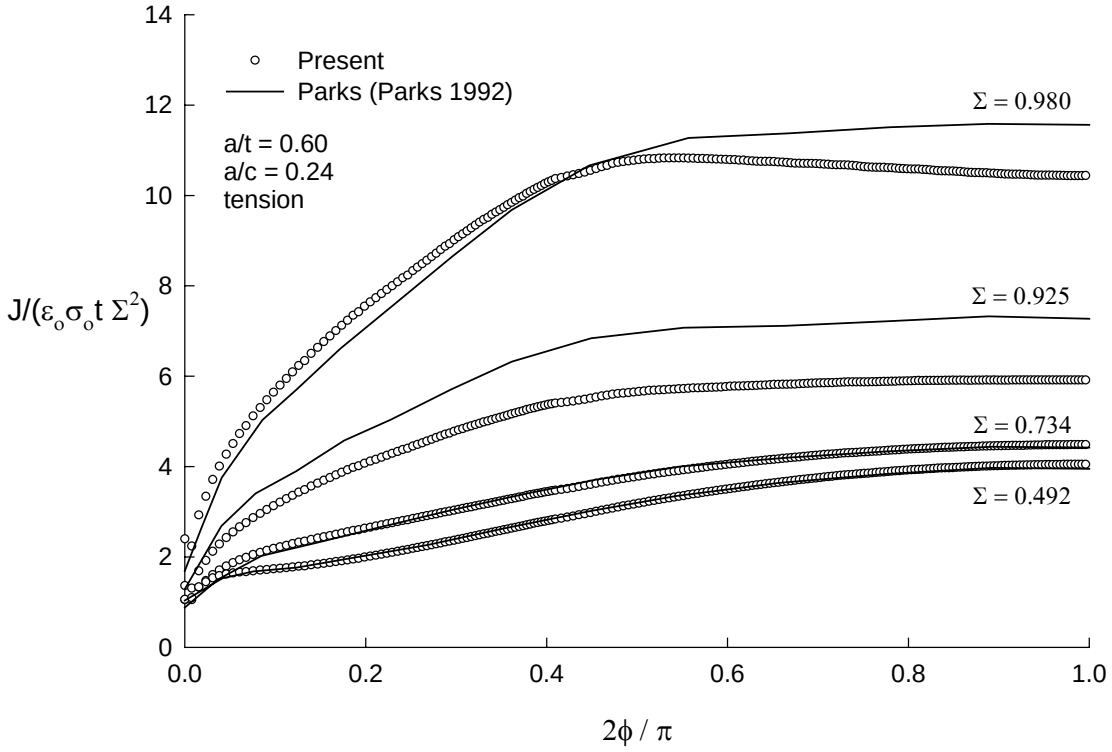

Figure 4-1.a *J*-integral Verification for Models Subjected to Tension

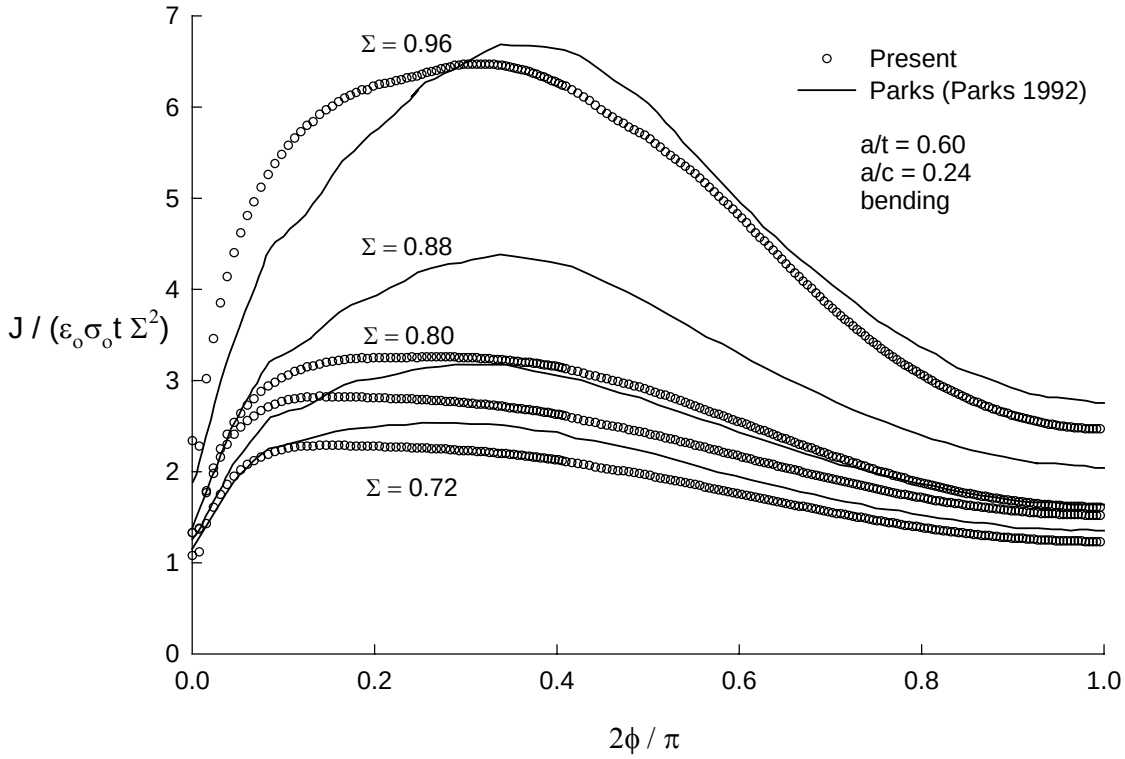

Figure 4-1.b *J*-integral Verification for Models Subjected to Bending

IV.B Material

Tensile tests were performed on the D6AC steel at INEEL on specimens cut in both the transverse and longitudinal rolling directions. The resulting material properties were essentially isotropic. The results from all tests were averaged to obtain a single value for use in the finite element analyses and are summarized in Table 4-1.

Table 4-1 Thiokol D6AC Steel Material Properties

Yield Stress, σ_o	1329.7 MPa
Ultimate Tensile Stress, σ_u	1434.0 MPa
Young's Modulus, E	209.7 GPa

An incremental plasticity, Ramberg-Osgood (Ramberg, 1943) material model was utilized in the finite element simulations. The Ramberg-Osgood model is defined by Eq. 4.1, where σ_o is the reference stress (yield stress), ε_o is the corresponding reference strain, n is the hardening exponent, and κ is the fitting constant.

$$\frac{\varepsilon}{\varepsilon_o} = \frac{\sigma}{\sigma_o} + \kappa\left(\frac{\sigma}{\sigma_o}\right)^n \tag{4-1}$$

Using this stress-strain relation, a Ramberg-Osgood stress strain curve was fit to the tensile test data. The input parameters used were σ_o = 1329.7 MPa, $\varepsilon_o = \sigma_o / E$, n = 50, and κ = 0.315. The curve-fit is presented in Figure 4-3 with the average tensile test data. Excellent agreement was obtained.

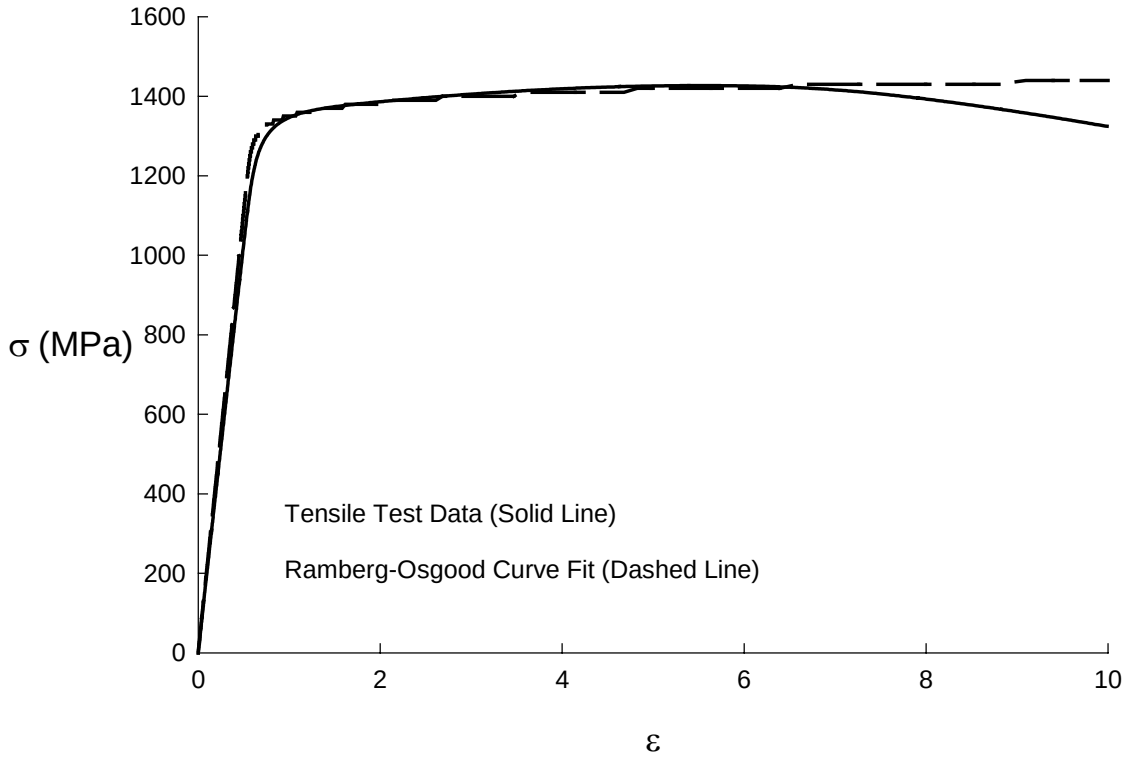

Figure 4-2 Ramberg-Osgood Curve Fit to Tensile Test Data

IV.C Analysis Specifications

The *l3disop* element type was used for the analyses. It is an 8-noded isoparametric element and employs a tri-linear displacement field (WARP3D, 2004). The WARP3D sparse solver was used in the analyses. Within the finite element code, the von-Mises yield criterion and its associated flow rule were used. Linear-kinematic element formulations (small strain) were used.

IV.D Boundary Conditions

The finite element model was constrained in a manner to simulate the symmetry planes of the surface crack (as outlined in Chapter 2). The *y*-*z* plane of the model was constrained in the *x*-direction and the un-cracked ligament on the crack plane was constrained in the *z*-direction. To prevent model translation, a single node located at the farthest point from the model origin (*(x, y, z) = (w, t, 0)*) was constrained in the *y*-direction.

IV.E Loading Specifications

The finite element models were loaded on the far face at $z = h$, in the *z*-direction. For the tensile cases, a uniform stress σ_T was applied on the element faces at this location, and for the bending cases, a linearly varying stress with σ_B at the upper surface *(y = t)* and $-\sigma_B$ at the lower surface *(y = 0)* was applied. The applied stresses for each specimen were equivalent to those presented in Tables 3-2a and 3-2b. The stresses were applied incrementally in 40 equal load steps, from zero to the maximum applied stress, in order to aid solution convergence.

IV.F Convergence Problems

Of the 14 tension and 8 bending models selected for analyses, two tension (AT-02, BT-04) and one bending model (BB-04) would not converge on a solution due to high levels of plasticity. These models are not considered in the presentation of results.

CHAPTER V

RESULTS AND DISCUSSION

V.A Constraint Calculations

The hyper-local constraint factor was calculated as a function of the parametric angle around the crack front for each surface crack model. A mathematical expression for the constraint calculation is shown in Equation 5.1.

$$\alpha(\phi) = \frac{1}{S(\phi)} \int_0^{S(\phi)} \left(\frac{\sigma_{zz}}{\sigma_o} \right) ds \tag{5-1}$$

Figure 5-1 provides a graphical representation of the path definition.

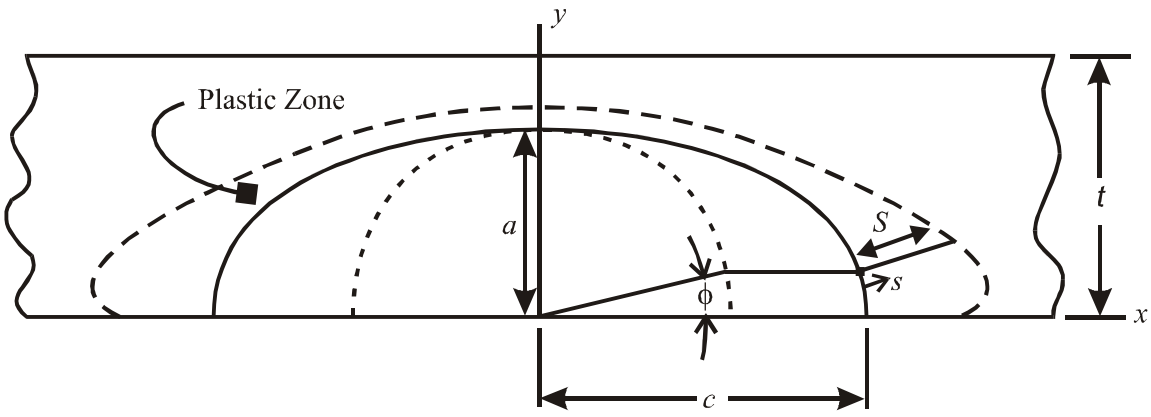

Figure 5-1 Constraint Path Definition

A FORTRAN routine ALPHAH was developed to calculate a constraint distribution for each surface crack model. The source code for ALPHAH is presented in Appendix A. The stress for each node on the crack plane

was taken as an average of the surrounding Gauss point stresses, and used as input for the routine. The nodes possessing a von-Mises stress greater than or equal to σ_o were used to define the plastic zone around the crack front. Each node lying on the crack front represents an individual ϕ value, as defined in Eq. 2.1, for which a constraint value is calculated. The yielded nodes which lie in a path perpendicular to the crack front *S* emanating from each crack front node are sorted into subsets, and average normal stress to flow stress ratio for each subset is considered as the α_h value for the corresponding ϕ. The hyper-local constraint factor distribution along the crack front is then plotted versus ϕ.

V.B *J*-Integral Calculations

FEA-Crack greatly simplified the calculation of the *J*-integral through automatic generation of WARP3D input files containing the appropriate *J* calculation commands. The domain integral method is used by WARP3D to calculate the *J*-integral (WARP3D, 2004). The average *J*-integral values for each ϕ location are output to a results file that is used to generate plots of *J* versus ϕ for each model. *J*-integral calculations were normalized by the product of the applied stress (σ_T or σ_B) and the thickness *t*.

V.C Fracture Initiation Location

The high-resolution fracture surface images provided by INEEL were analyzed to determine the location along the crack front that exhibited the largest amount of crack extension. This is an arduous task and is highly subject to the interpretation of the

analyst. Each fracture surface image was digitized, and the ϕ location of maximum crack extension on both sides of the initial surface crack was visually selected and recorded. Figure 5-2[2] shows a typical fracture surface and corresponding ϕ locations. The two ϕ values were then averaged to obtain a single location of maximum crack extension for each test specimen. The point of maximum crack extension is considered the fracture initiation location, and will be used to validate the developed fracture criterion.

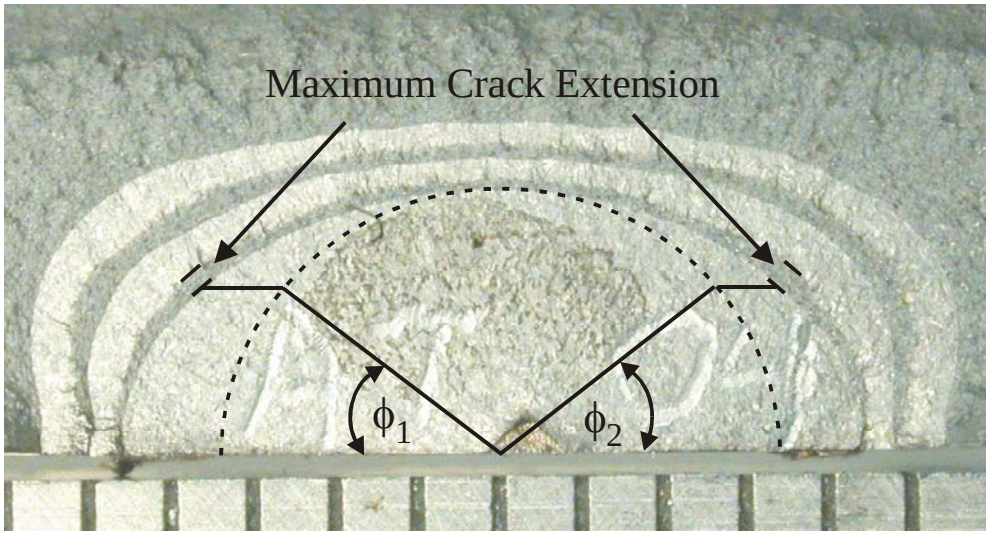

Figure 5-2 Typical Maximum Crack Extension Location Measurement

[2] Note that in the figure shown, the crack did not grow symmetrically around the EDM notch, implying that it may not have been in the center of the specimen.

V.D Discussion of Results

Surface cracks under tension and bending possess different characteristic crack front stress fields. *J*-integral and constraint calculations for tension and bending thus differ in characteristic shape. The shape of each curve is related to the plastic zone size around the crack front. The *J*-integral signifies the extent of stress and strain elevation along the crack front, so it shares a direct relationship with the amount of crack extension present. Conversely, increased plasticity signifies a loss of constraint; hence, constraint and plastic zone size exhibit an indirect relationship. The calculated α_h and *J*-integral distributions were plotted for each model as well as the product $J\alpha_h$ normalized in the same fashion as the *J*-integral. A comprehensive set of plots for each crack configuration and loading type is presented in Appendix B.

V.D.1 Tension Specimen *J*-integral and α_h Distributions

The *J*-integral and constraint variation around a monotonically tensile loaded surface crack front share the same typical shape. The plastic zone of a surface crack under tension appears as a bulge just beneath the free surface, and decreases to a constant value as the deepest point of penetration is approached. The *J*-integral and α_h distributions mimic this as both display a steep gradient just below the free surface at small values of ϕ and approach a constant value towards $\phi = \pi / 2$. A typical variation of the *J*-integral and α_h distributions for a surface crack loaded under tension is shown in Figure 5-3.

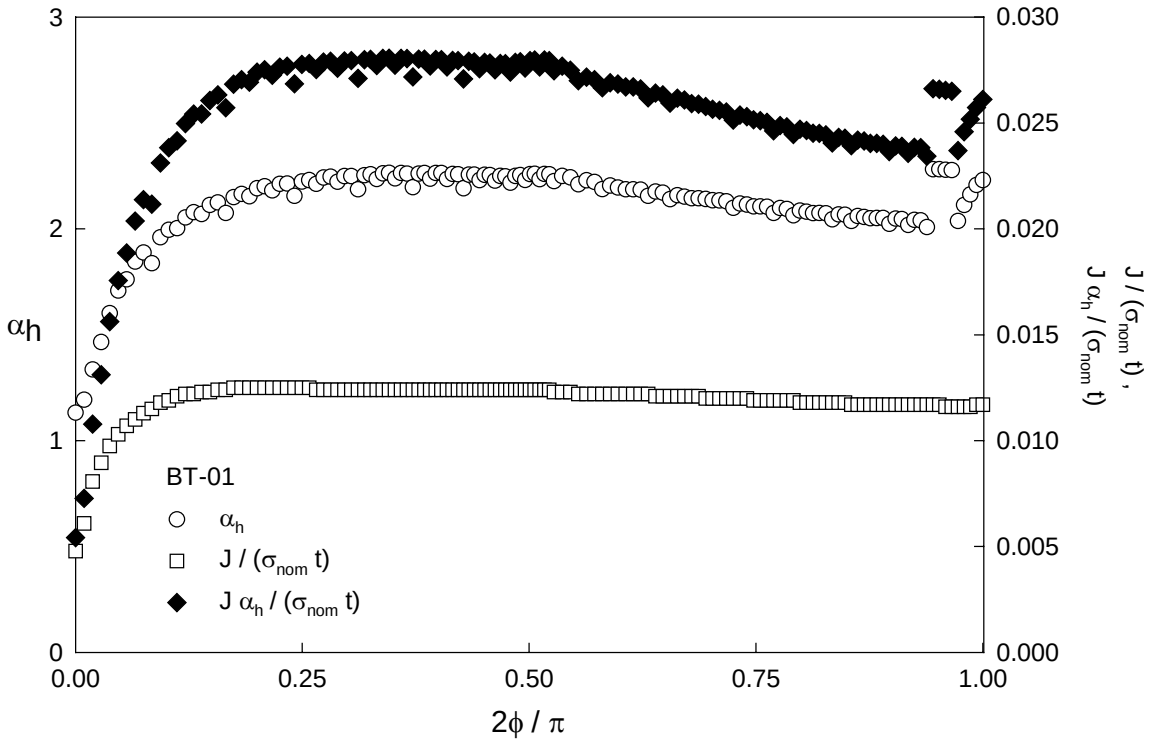

Figure 5-3.a Typical *J* and α_h Distribution along the Surface Crack Front (Tension) (a = 4.27 mm, c = 6.97 mm)

V.D.2 Bending Specimen *J*-integral and α_h Distributions

The stress fields in a surface crack subjected to bending promote a large plastic zone at a distance below the free surface of the crack and a much smaller plastic zone towards the deepest point of penetration. The stress gradients along the crack front are more severe than in tension specimens as evidenced in the characteristic *J*-integral and α_h values along the crack front. *J* values reach a maximum value where the plastic zone is largest and rapidly decrease with the plastic zone size; however, towards the deepest point of penetration constraint calculations for surface crack bend specimens tend to show much smaller variations along the crack front and reach a maximum value where the plastic

zone is the smallest. A typical surface crack J and α_h plot for a model loaded under bending is provided in Figure 5-3.b.

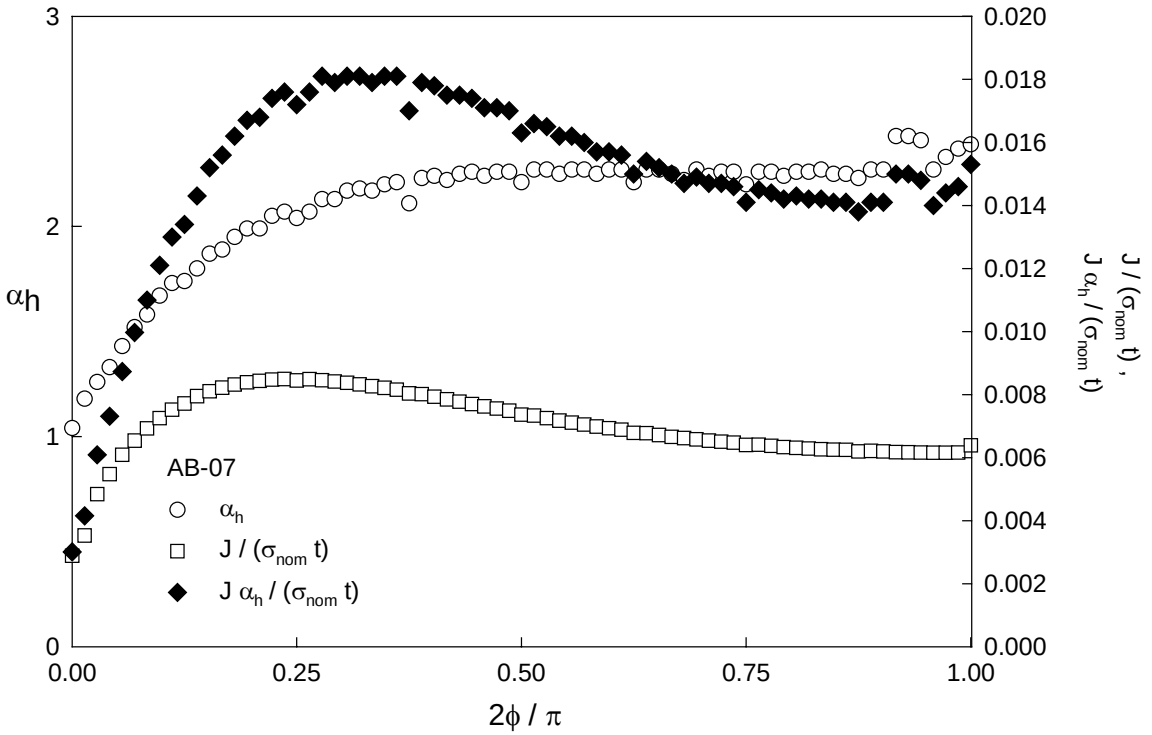

Figure 5-3.b Typical J and α_h Distribution along the Surface Crack Front (Bending) (a = 1.516 mm, c = 1.822 mm)

V.E Fracture Prediction

The proposed fracture criterion is intended to recognize the location of maximum crack extension as the point of highest $J\alpha_h$ along the crack front. The ϕ location of maximum $J\alpha_h$, denoted as ϕ_{crit} *predicted* was plotted against the critical ϕ location taken from the fracture surface images, ϕ_{crit} *measured* for both the tension and bending cases. Figures 5-4.a and 5-4.b show the tension and bending comparisons, respectively. A one-to-one correspondence indicates perfect agreement between the measured and predicted

critical location. Some test specimens did not exhibit enough crack extension to obtain the critical location. These were not included in the comparison.

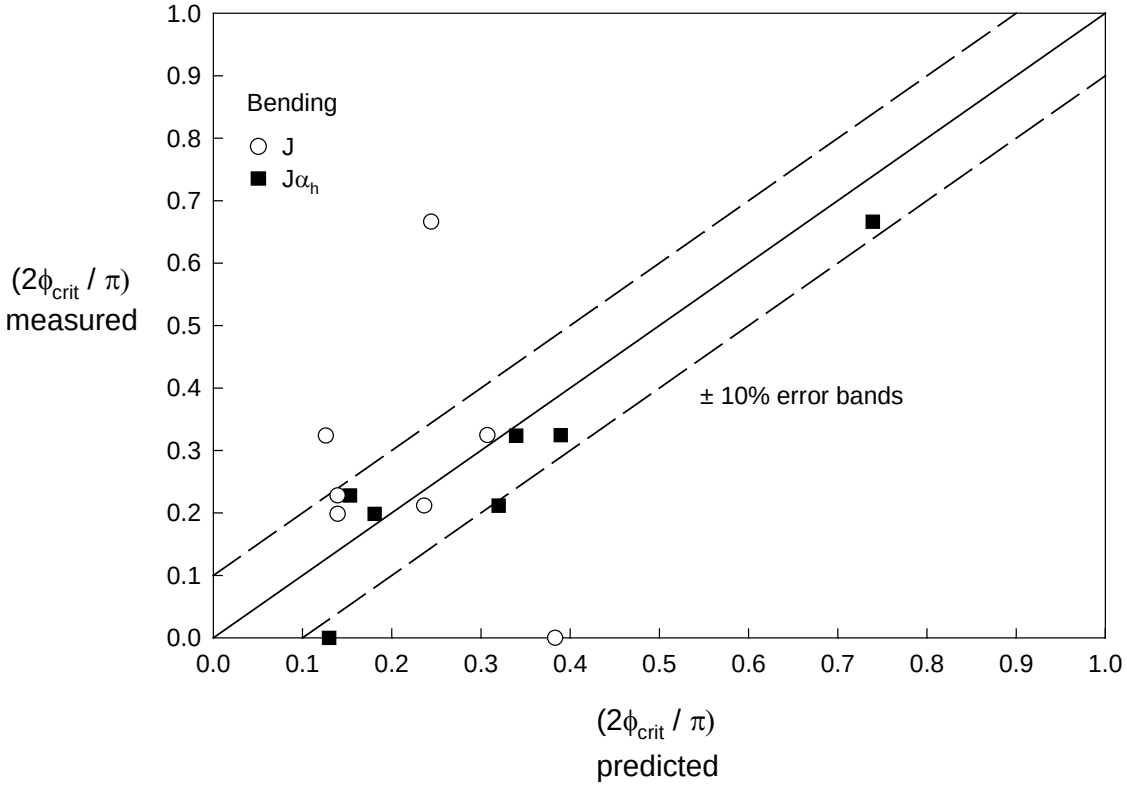

Figure 5-4.a Comparison of Predicted and Measured Critical Location (Bending)

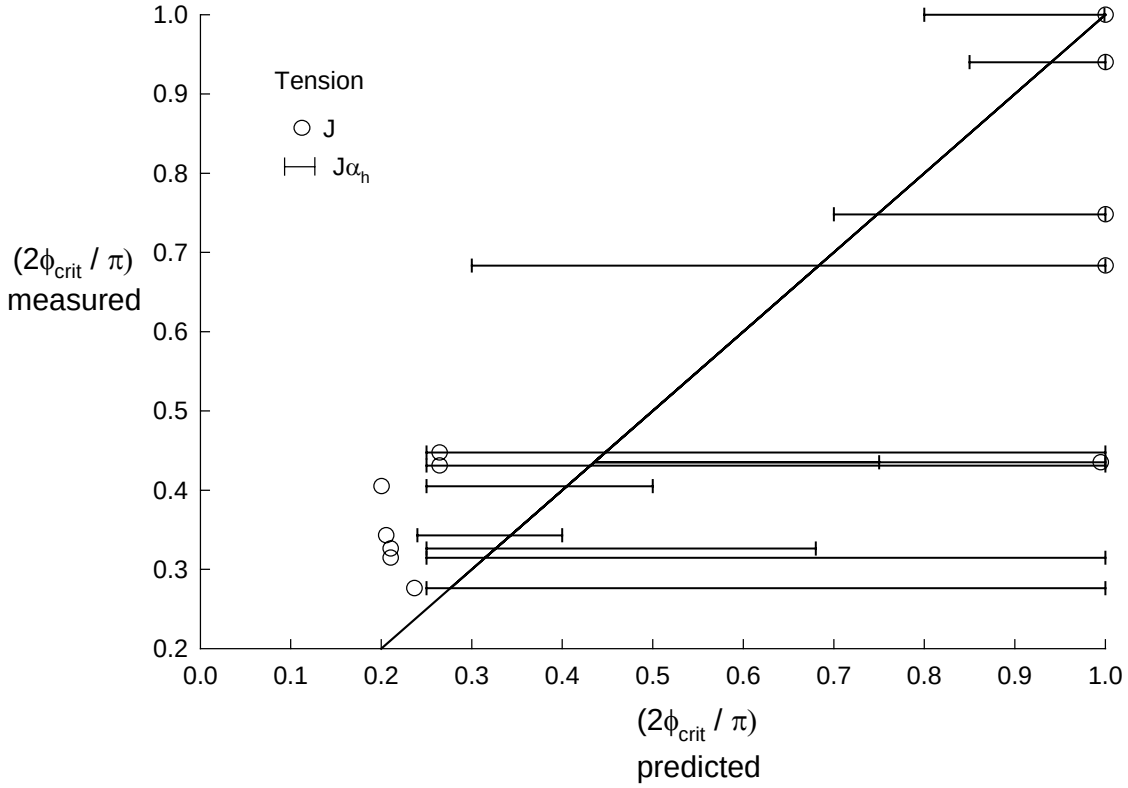

Figure 5-4.b Comparison of Predicted and Measured Critical Location (Tension)

V.F Crack Extension

A correlation between the crack extension normal to and along the crack front and the $J\alpha_h$ distributions was observed for both the tension and the bending specimens. This relationship provides further evidence to the validity of the proposed fracture criterion. To observe the relation, the crack extension was digitized and recorded for corresponding values of ϕ along the crack front. The data was then plotted alongside the $J\alpha_h$ distribution from the appropriate specimen. Sample tension and bending correlation examples are presented in Figures 5-5.a and 5-5.b. The cases considered for crack extension correlation to $J\alpha_h$ are given in Appendix C.

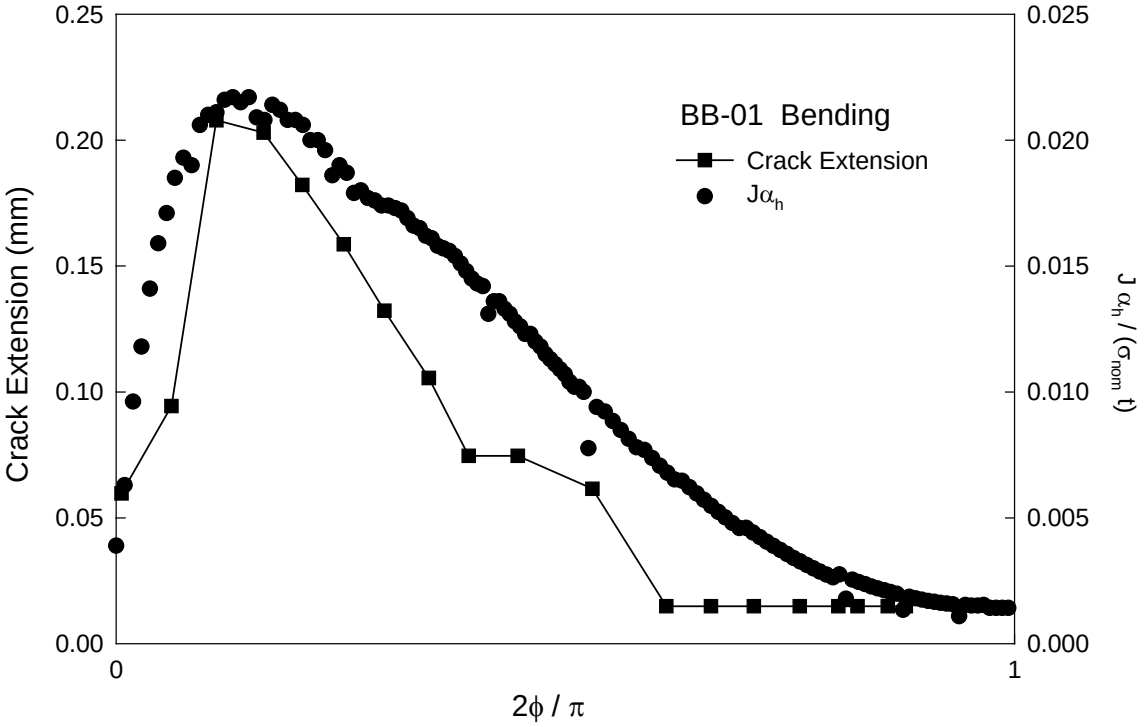

Figure 5-5.a Sample Crack Extension Correlated with $J\alpha_h$ (Bending)

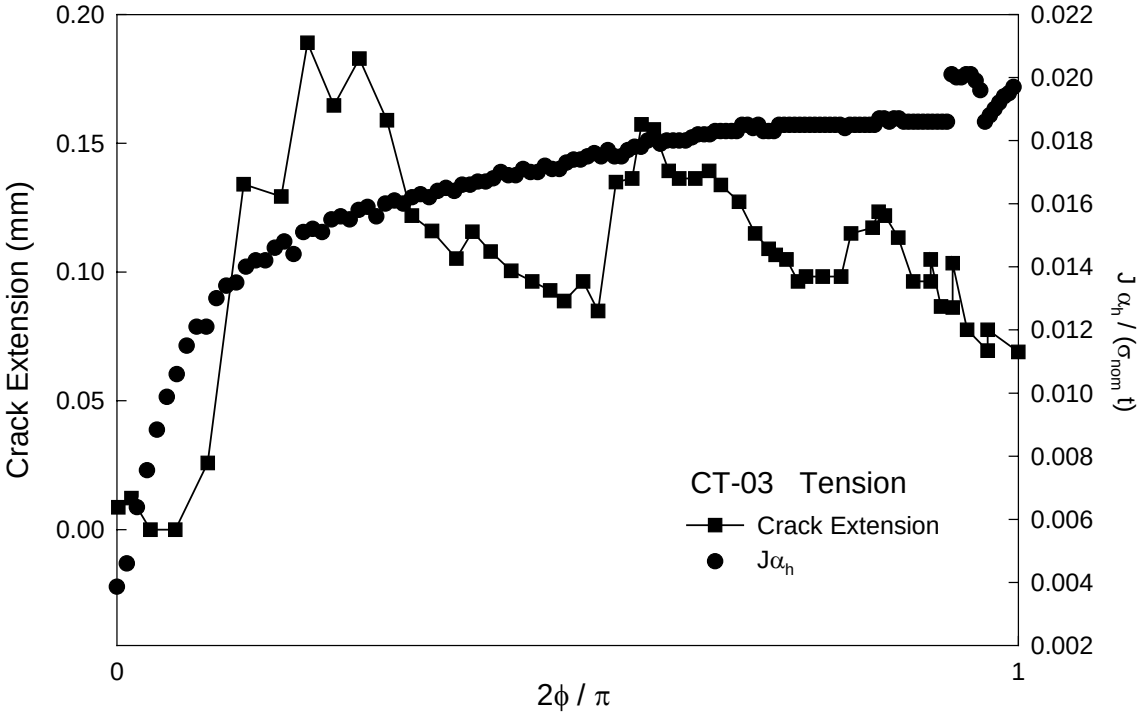

Figure 5-5.b Sample Crack Extension Correlated with $J\alpha_h$ (Tension)

CHAPTER VI

CONCLUSIONS AND FUTURE WORK

VI.A Fracture Prediction Validity

The use of $J\alpha_h$ as a fracture prediction criterion for ductile materials is promising. For the case of a surface crack under bending, the criterion predicted the critical location within approximately 10% error for all specimens considered. For surface cracks under tension, the criterion was inconclusive. The results presented for tension showed little variation of $J\alpha_h$ along the crack front in the critical regions, thus a single location of maximum $J\alpha_h$ could not be identified. Thus, crack initiations could occur at $2\phi/\pi$ from 0.25 to 1.0. However, for the tension specimens analyzed, the measured critical location fell within the range of constant $J\alpha_h$ for all considered cases implying that the criterion has not been disproved by these results.

VI.B Suggested Future Work

A rigorous validation of the fracture criterion should be conducted before widespread use is considered. Replicate surface cracked specimens of identical crack size and applied loading would prove useful in confirming the data presented herein. In addition to the application of the criterion to surface cracked geometries, the use of the

hyper-local constraint factor as a normalization relating different crack configurations would prove invaluable for future development.

REFERENCES

Ayres, 1970 — Ayres, D. J., "A Numerical Procedure For Calculating Stress and Deformation Near a Slit In a Three-Dimensional Elastic-Plastic Solid," *Engineering Fracture Mechanics*, Vol. 2, 1970, pp. 87-106.

Aveline, 1999 — Aveline, C. R., Jr. and Daniewicz, S. R., "Variations of Constraint and Plastic Zone Size in Surface-Cracked Plates Under Tension or Bending Loads," *Fatigue and Fracture Mechanics: 31st Volume, ASTM STP 1389*, G. R. Halford and J. P. Gallagher, Eds., American Society for Testing and Materials, West Conshohocken, PA, 2000, pp. 206-220.

Dodds, 1993 — Dodds, R. H., Jr., Shih, C. F. and Anderson, T. L., "Continuum and Micromechanics Treatment of Constraint in Fracture," *International Journal of Fracture*, Vol. 64, 1993, pp. 101-133.

Faleskog, 1995 — Faleskog, J., "Effects of Local Constraint Along Three-Dimensional Crack Fronts-A Numerical and Experimental Investigation," *Journal of the Mechanics and Physics of Solids*, Vol. 43, No.3, 1995, pp. 447-493.

Fawaz, 2004 — Fawaz, S. A. and Andersson, B., "Accurate Stress Intensity Factor Solutions for Corner Cracks at a Hole," *Engineering Fracture Mechanics*, Vol. 71, 2004, pp. 1235-1254.

Gao, 1998 — Gao, X., Faleskog, J., Shih, C.F. and Dodds, R.H., Jr., "Ductile Tearing in Part-Through Cracks: Experiments and Cell-Model Predictions," *Engineering Fracture Mechanics*, Vol. 59, No. 6, 1998, pp. 761-777.

Griffith, 1920 — Griffith, A. A., "The Phenomena of Rupture and Flow of Solids," *Philosophical Transactions of Royal Society*, Vol. A-221, 1920, p. 163.

Hancock, 1976	Hancock, J. W. and Mackenzie, A. C., "On The Mechanisms of Ductile Failure in High-Strength Steels Subjected to Multi-Axial Stress-States," *Journal of the Mechanics and Physics of Solids*, Vol. 24, 1976, pp. 147-169.
Hancock, 1991	Hancock, J. W., Reuter, W. G. and Parks, D. M., "Constraint and Toughness Parameterized by *T*," ASTM Symposium on Constraint Effects in Fracture, Indianapolis, IN, 1991.
Hult, 1956	Hult, J. A. H. and McClintock, F. A., "Elastic-Plastic Stress and Strain Distribution Around Sharp Notches Under Repeated Shear," *Proceedings of the 9th International Congress on Applied Mechanics*, Brussels, Belgium, 1956.
Irwin, 1956	Irwin, G. R., "Relation of Stresses Near a Crack to the Crack Extension Force," *Proceedings of the 9th International Congress on Applied Mechanics*, Brussels, Belgium, 1956.
Irwin, 1962	Irwin, G. R., "The Crack Extension Force for a Part Through Crack in a Plate," *Journal of Applied Mechanics*, Vol. 29, No. 4, 1962, pp. 651-654.
Levy, 1971	Levy, N., Marcal, P.V. and Rice, J.R., "Progress in Three-Dimensional Elastic-Plastic Stress Analysis for Fracture Mechanics," *Nuclear Engineering and Design*, Vol. 17, 1971, pp. 64-75.
McClintock, 1968	McClintock, F. A., "A Criterion for Ductile Fracture by the Growth of Holes," *Journal of Applied Mechanics, Vol. 35, 1968, pp. 363-371*.
McMeeking, 1979	McMeeking, R. M. and Parks, D. M., "On Criteria for J-Dominance of Crack Tip Fields in Large Scale Yielding," ASTM STP 668, pp. 1750-194, 1979.
Newman, 1981	Newman, J. C., Jr. and Raju, I. S., "An Empirical Stress-Intensity Factor Equation for the Surface Crack," *Engineering Fracture Mechanics*, Vol. 15, No. 1-2, 1981, pp. 185-192.
Newman, 1993	Newman, J.C., Jr., Bigelow, C.A. and Shivakumar, K.N., "Three-Dimensional Elastic-Plastic Finite-Element Analyses of Constraint Variations in Cracked Bodies," *Engineering Fracture Mechanics*, Vol. 46, No. 1, 1993, pp. 1-13.

Newman, 1995 — Newman, J.C., Jr., Crews, J.H., Jr., Bigelow, C.A., and Dawicke, D.S., "Variation of a Global Constraint Factor in Cracked Bodies Under Tension and Bending Loads," *Constraint Effects in Fracture Theory and Applications: Second Volume, ASTM STP 1244*, Mark Kirk and Ad Bakker, Eds., American Society for Testing and Materials, Philadelphia, 1995.

Newman, 1999 — Newman, J.C., Jr., Reuter, W.G., and Aveline, C.R., Jr., "Stress and Fracture Analyses of the Surface Crack," *Fatigue and Fracture Mechanics: 30th Volume, ASTM STP 1360*, K. L. Jerina and P. C. Paris, Eds., American Society for Testing and Materials, Philadelphia, PA, 1999.

Newman, 2000 — Newman, J. C., Jr., "Irwin's Stress Intensity Factor – A Historical Perspective," *Fatigue and Fracture Mechanics: 31st Volume, ASTM STP 1389*, G. R. Halford and J. P. Gallagher, Eds., American Society for Testing and Materials, West Conshohocken, PA, 2000, pp. 39-53.

O'Dowd, 1991 — O'Dowd, N. P. and Shih, C. F., "A Family of Crack Tip Fields Characterized by a Triaxiality Paramater Part I – Structure of Field," *Journal of the Mechanics and Physics of Solids*, Vol. 39, 1991, pp. 989-1015.

Parks, 1992 — Parks, D. M., "Advances in Characterization of Elastic-Plastic Crack-Tip Fields," *Topics in Fracture and Fatigue*, A. S. Argon, Ed., 1992.

Ramberg, 1943 — Ramberg, W. and Osgood, WR, "Description of Stress-strain Curves by Three Parameters," NACA Tech. Note, 902, 1943.

Raju, 1979 — Raju, I. S. and Newman, J. C., Jr., "Stress Intensity Factors for a Wide Range of Semi-Elliptical Surface Cracks in Finite-Thickness Plates," *Engineering Fracture Mechanics*, Vol. 11, 1979, pp. 817-829.

Reuter, 1994 — Reuter, W. G., Newman, J. C., Jr., Macdonald, B. D., and Powell, S. R., "Fracture Criteria for Surface Cracks in Brittle Materials," *Fracture Mechanics: 24th Volume, ASTM STP 1207*, J. D. Landes, D. E., Mccabe, and J. A. M. Boulet, Eds., American Society for Testing and Materials, Philadelphia, PA, 1994, pp. 617-635.

Reuter, 2002 — Reuter, W. G., Newman, J. C., Jr., Skinner, J. D., Mear, M. E. and Lloyd, W. R., "Use of K_{IC} and Constraint to Predict Load and Location for Initiation of Crack Growth in Specimens Containing Part-Through Cracks," *Fatigue and Fracture Mechanics: 32nd Volume, STP 1406*, R. Chona, Ed., American Society for Testing and Materials, West Conshohocken, PA, 2002, pp. 353-380.

Rice, 1968 — Rice, J. R., "A Path Independent Integral and the Approximate Analysis of Strain Concentration by Notches and Cracks," *Journal of Applied Mechanics*, Vol. 35, 1968, pp. 379-386.

Rice, 1969 — Rice, J. R. and Tracey, D. M., "On the Ductile Enlargement of Voids in Triaxial Stress Fields," *Journal of the Mechanics and Physics of Solids*, Vol. 17, 1969, pp. 201-217.

Shih, 1981 — Shih, C. F. and German, M. D., "Requirements for a One Parameter Characterization of Crack Tip Fields by the HRR Singularity," *International Journal of Fracture*, Vol. 17, 1981, pp. 27-43.

Sommer, 1991 — Sommer, E. and Aurich, D., "On the Effect of Constraint on Ductile Fracture," *Defect Assessment in Components – Fundamentals and Applications*, ESIS/EGF9, J. G. Blauel and K. H. Schwalbe, Eds., 1991, Mechanical Engineering Publications, London, pp. 141-174.

Timoshenko, 1970 — Timoshenko, S. P., and Goodier, J. N., *Theory of Elasticity*, McGraw-Hill, New York, 1970.

Trantina, 1983 — Trantina, G.G., deLorenzi, H.G. and Wilkening, W.W., "Three-Dimensional Elastic-Plastic Finite Element Analysis of Small Surface Cracks," *Engineering Fracture Mechanics*, Vol. 18, No. 5, 1983, pp. 925-938.

WARP3D, 2004 — Gullerud, A. S., Koppenhoefer, K. C., Roy, A., RoyChowdhury, S., Walters, M. C. and Dodds, R. H., Jr., WARP3D – Release 15 Manual. Civil Engineering, Report No. UILU-ENG-95-2012m University of Illinois at Urbana-Champaign, Urbana, IL, 2004.

Williams, 1957 — Williams, M. L., "On the Stress Distribution at the Base of a Stationary Crack," *Journal of Applied Mechanics*, Vol. 24, 1957, pp. 109-114.

APPENDIX A

FORTRAN PROGRAM ALPHAH.F90

CONSTRAINT POSTPROCESSING ROUTINE

```
program ALPHAH

implicit none

real::xcoord,ycoord,zcoord,filestatus,min,ra,rra,distmin,dist,r0,y0,x0,y,x,&
       xdif,ydif,x1,x2,y1,y2,sx,sy,sz,sxy,syz,sxz,Uo,svm,temp,flos,c,a,w,t,l,da_x,&
    tol,aa,bb,cc,counter2,wtsum,ctrad,rad_dist,toler,m
integer::i,cmax,bcmax,null1,n,nodeno,NodeMax,j,k,ir,kk,counter,Elemno,n1,n2,n3,n4,&
      n5,n6,n7,n8,ElemMax,ngpt,step,elem,gpt,ii,status


real,dimension(:,:),allocatable::crack,crackinit,bcrack,bcrackinit,d,crack1,crack2,&
                  Node,stress,stravg,alpha
real,dimension(:),allocatable::GptStrz,GptStrvm,zstress,wtstrz,wt
integer,dimension(:),allocatable::crackmask,bcmask,pzmask,gptmask
integer,dimension(:,:),allocatable::cfnmask,element,Const

!Open Input Files

  open (10, file='crack.crd')
  open (11, file='belowcrack.crd')
  open (12, file='nodes.crd')
  open (13, file='elements.elm')
  open (14, file = 'stress.out', STATUS='OLD', ACTION='READ', IOSTAT=status)

!Open Output Files

  open (20, file = 'test.out')
  open (21, file = 'pzone.crd')
  open (22, file = 'constraint.txt')

!Input Variables

  flos=1329.7
  c=4.445          !crack length
  a=-3.2          !crack depth
  w=25.4           !model width
  t=6.350          !model thickness
  l=50.8          !model length
  da_x=1.7066660000E-02       !distance between adjacent nodes in crack tube
  tol=.0009        !tolerance required to select crack front ellipse
  ctrad=0.01       !crack tube radius

!Initialize Nodal Coordinate Array to set NodeMax

  n=0
  do while (filestatus.ge.0)
    read(12,40,iostat=filestatus) Nodeno,xcoord,ycoord,zcoord
40  format (I8,3F17.8)
    n=n+1
  enddo
  n=n-1
  NodeMax=0
```

```
  NodeMax=n
  filestatus=0
  rewind(12)

!Build Nodal Array

  allocate(Node(NodeMax,4))
  do i=1,NodeMax
    read(12,*,iostat=filestatus) Nodeno,xcoord,ycoord,zcoord
    Node(i,1)=Nodeno
    Node(i,2)=xcoord
    Node(i,3)=ycoord
    Node(i,4)=zcoord
  enddo
  filestatus=0

!Initialize Element Array
  n=0
  do while (filestatus.ge.0)
    read(13,50,iostat=filestatus) Elemno,n1,n2,n3,n4,n5,n6,n7,n8
50 format (9I8)
    n=n+1
  enddo
  n=n-1
  ElemMax=0
  ElemMax=n
  filestatus=0
  rewind(13)

!Build Element Array

  allocate(Element(n,9))
  do i=1,ElemMax
    read(13,50,iostat=filestatus) Elemno,n1,n2,n3,n4,n5,n6,n7,n8
    Element(i,1)=Elemno
    Element(i,2)=n1
    Element(i,3)=n2
    Element(i,4)=n3
    Element(i,5)=n4
    Element(i,6)=n5
    Element(i,7)=n6
    Element(i,8)=n7
    Element(i,9)=n8
  enddo

!Initialize Crack Array to set Cmax (number of crack front nodes)

  n=0
  do while(filestatus.ge.0)
    n=n+1
    read(10,*,iostat=filestatus) NULL1,Nodeno,xcoord,ycoord,zcoord
  enddo
  cmax=n-1
```

```
  filestatus=0
  rewind(10)

!Build Initial Crack Array

  allocate(crackinit(cmax,4))
30 format(A4,I8,1x,E15.6,1x,E15.6,1x,E15.6)
  do i=1,cmax
    read(10,30,iostat=filestatus) NULL1,Nodeno,xcoord,ycoord,zcoord
    crackinit(i,1)=nodeno
    crackinit(i,2)=xcoord
    crackinit(i,3)=ycoord
    crackinit(i,4)=zcoord
  enddo
  filestatus=0


!Initialize Below Crack Array to set bcmax (number of nodes on and below the crack front)

  n=0
  do while(filestatus.ge.0)
    n=n+1
    read(11,*,iostat=filestatus) NULL1,nodeno,xcoord,ycoord,zcoord
  enddo
  filestatus=0
  bcmax=n-1
  rewind(11)

!Build Initial Below Crack Array

  allocate(bcrackinit(bcmax,4))
  do i=1,bcmax
    read(11,30,iostat=filestatus) NULL1,nodeno,xcoord,ycoord,zcoord
    bcrackinit(i,1)=nodeno
    bcrackinit(i,2)=xcoord
    bcrackinit(i,3)=ycoord
    bcrackinit(i,4)=zcoord
  enddo

!Fill Crack Front Mask Array and Crack Node/Coordinate Array

  allocate(crackmask(NodeMax))
  allocate(crack(Nodemax,4))
  do i=1,cmax
    do j=1,NodeMax
      if (int(crackinit(i,1)).eq.j) then
        crackmask(j)=1
        crack(j,1)=j
        crack(j,2)=crackinit(i,2)
        crack(j,3)=crackinit(i,3)
        crack(j,4)=crackinit(i,4)
      endif
    enddo
```

```
  enddo


!Fill Below Crack Mask Array and Node/Coordinate Array

  allocate(bcmask(NodeMax))
  allocate(bcrack(NodeMax,4))
  do i=1,bcmax
    do j=1,NodeMax
      if (int(bcrackinit(i,1)).eq.j) then
          bcmask(j)=1
          bcrack(j,1)=j
          bcrack(j,2)=bcrackinit(i,2)
          bcrack(j,3)=bcrackinit(i,3)
          bcrack(j,4)=bcrackinit(i,4)
      endif
    enddo
  enddo


!Using the crack front array which contains all the nodes on the actual crack front
!and the below crack array, which contains the nodes below the crack front,
!determine which node is the shortest distance from each crack front node,
!and store in the array crack 2. The result will be an array of nodes which form a
!concentric ellipse to the crack front

k=1
allocate(d(NodeMax,2))
allocate(crack2(cmax,3))

do i=1,NodeMax
          distmin=99999
          if (crackmask(i).eq.1) then    !if node is on crack front
                    do j=1,NodeMax
                              if (bcmask(j).eq.1) then   !if node is below crack front
                        if (int(crack(i,1)).ne.int(bcrack(j,1))) then
                                                  dist=sqrt(((bcrack(j,2)-crack(i,2))**2)+((bcrack(j,3)-
                                                        crack(i,3))**2))
          if (dist.lt.distmin) then
            distmin=dist
            NodeNo=j
          endif
         endif
       endif
    enddo
    d(k,1)=NodeNo
    d(k,2)=distmin
    k=k+1
  endif
enddo
k=k-1

do i=1,cmax
```

```
            crack2(i,1)=d(i,1)
  crack2(i,2)=bcrack(d(i,1),2)
  crack2(i,3)=bcrack(d(i,1),3)
enddo
allocate(crack1(cmax,3))
kk=1

do i=1,NodeMax
  if (crackmask(i).eq.1) then
              crack1(kk,1)=crack(i,1)
    crack1(kk,2)=crack(i,2)
    crack1(kk,3)=crack(i,3)
    kk=kk+1
  endif
enddo
kk=kk-1

!call sort_pick(crack1)

do j=3,k
  aa=crack1(j,3)
  bb=crack1(j,1)
  cc=crack1(j,2)
  do i=j-1,1,-1
    if (crack1(i,3) <= aa) exit
    crack1(i+1,1)=crack1(i,1)
    crack1(i+1,3)=crack1(i,3)
    crack1(i+1,2)=crack1(i,2)
  enddo
  crack1(i+1,3)=aa
  crack1(i+1,1)=bb
  crack1(i+1,2)=cc
enddo

!call sort_pick(crack2)

do j=3,k
  aa=crack2(j,3)
  bb=crack2(j,1)
  cc=crack2(j,2)
  do i=j-1,1,-1
    if (crack2(i,3) <= a) exit
    crack2(i+1,1)=crack2(i,1)
    crack2(i+1,3)=crack2(i,3)
    crack2(i+1,2)=crack2(i,2)
  enddo
  crack2(i+1,3)=aa
  crack2(i+1,1)=bb
  crack2(i+1,2)=cc
enddo
```

```
!Determine which nodes lie in rays 'normal' to the crack front

allocate(cfnmask(NodeMax,cmax))
do i=1,k
  do j=1,NodeMax
    if (bcmask(j).eq.1) then
      x2=crack2(i,2)
      y2=crack2(i,3)
      x1=crack1(i,2)
      y1=crack1(i,3)
      if (x2-x1.ne.0) then
                                          X=bcrack(j,2)
        Y=bcrack(j,3)
        m=((y2-y1)/(x2-x1))
        toler=m*(X-x1)+y1-Y
        toler=abs(toler)
        if (toler.le.da_x) then
          cfnmask(j,i)=1
        else
          cfnmask(j,i)=0
        endif
      else
        Y=bcrack(j,3)
        x=x2-(((y2-Y)*(x2-x1))/(y2-y1))
        xdif=abs(bcrack(j,2)-x)
        if (xdif.le.0.00001) then
          cfnmask(j,i)=1
        else
          cfnmask(j,i)=0
        endif
      endif
    endif
  enddo
enddo

!Read in results to determine which nodes are yielded

          ngpt=ElemMax*8
100 format (1x,i5,1x,i5,1x,i5,2x,8e14.6)

do
  read (14,*, IOSTAT=status) temp
  if (status /=0) exit
enddo
rewind(14)

allocate(stress(ngpt,4),STAT=status)
allocate(gptmask(ngpt))

do i=1,ngpt
  read(14,100) step,elem,gpt,sx,sy,sz,sxy,syz,sxz,Uo,svm
  stress(i,1)=elem
  stress(i,2)=gpt
```

```
  stress(i,3)=sz
  stress(i,4)=svm
  gptmask(i)=1
enddo


allocate(GptStrz(NodeMax))
allocate(GptStrvm(NodeMax))
allocate(StrAvg(NodeMax,3))

do j=1,NodeMax
  counter2=0
  do i=1,ngpt
                    if (gptmask(i).eq.1) then
      if (int(stress(i,2)).eq.j) then
        counter2=counter2+1
                GptStrz(counter2)=stress(i,3)
        GptStrvm(counter2)=stress(i,4)
        gptmask(i)=0
      endif
    endif
          enddo
          StrAvg(j,1)=j
          StrAvg(j,2)=sum(GptStrz)/counter2
  StrAvg(j,3)=sum(GptStrvm)/counter2
  do k=1,NodeMax
    GptStrz(k)=0
    GptStrvm(k)=0
  enddo
enddo

allocate(Const(NodeMax,3))

do i=1,NodeMax
  Const(i,1)=Node(i,1)
  if (Node(i,4).eq.0) then
    Const(i,3)=1
  else
    Const(i,3)=0
  endif
enddo

allocate(pzmask(NodeMax))

do i=1,NodeMax
  if (bcmask(i).eq.1) then
    if (StrAvg(i,3).ge.flos) then
      pzmask(i)=1
    else
      pzmask(i)=0
    endif
  endif
enddo
```

```
do i=1,NodeMax
  if (pzmask(i).eq.1) then
120 format (I8,4F17.8)
            write (21,120) int(Node(i,1)), Node(i,2), Node(i,3), Node(i,4), StrAvg(i,2)
  endif
enddo

allocate(zstress(NodeMax))
allocate(alpha(cmax,2))
allocate(wt(NodeMax))
allocate(wtstrz(NodeMax))

do i=1,cmax
  counter2=0
  do j=1,NodeMax
    zstress(j)=0
    if (cfnmask(j,i).eq.1) then
      if (pzmask(j).eq.1) then
        counter2=counter2+1
        zstress(j)=StrAvg(j,2)
      endif
    endif
  enddo
  alpha(i,1)=asin(abs(crack1(i,3))/abs(a))
  alpha(i,2)=(abs(sum(zstress)/counter2))/flos
enddo


130 format (3E14.6)

do i=1,cmax
  write (22,130) alpha(i,1), alpha(i,2)
enddo

end ALPHAH
```

APPENDIX B.1

J-INTEGRAL AND α_h VARIATIONS

RESULTS – TENSION

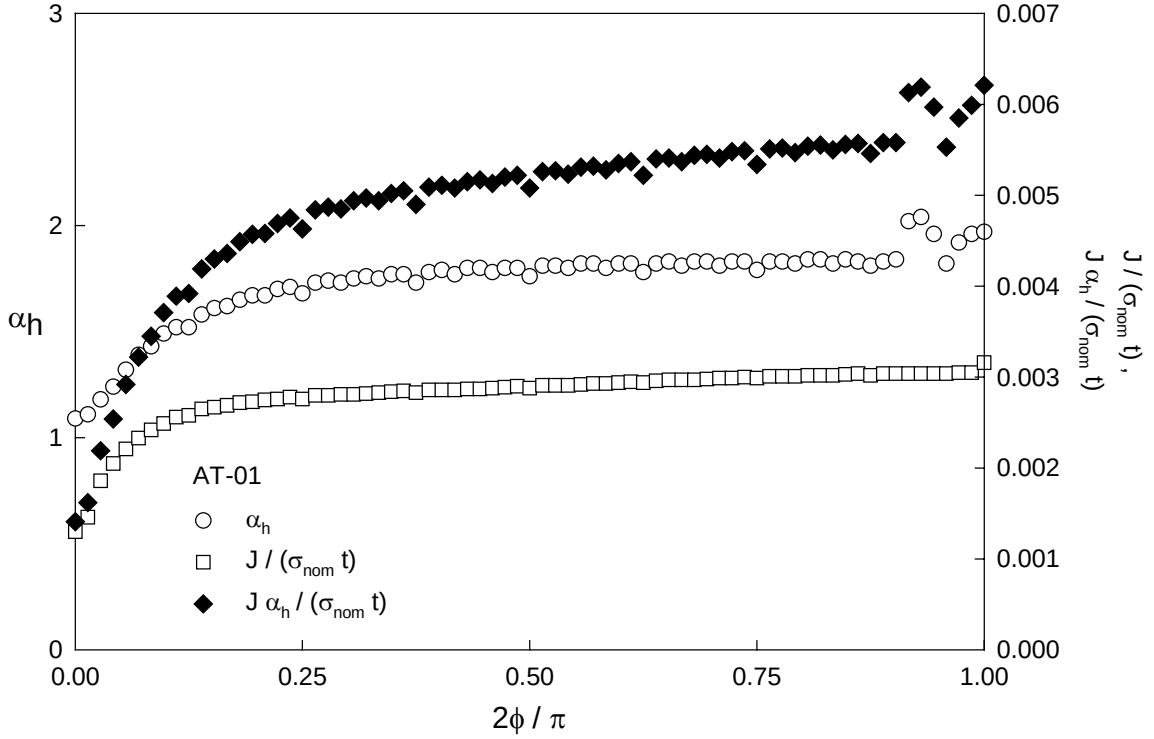

Figure B.1-1 AT-01 *J* and α_h Distribution (a = 1.22 mm, c = 1.6 mm, tension)

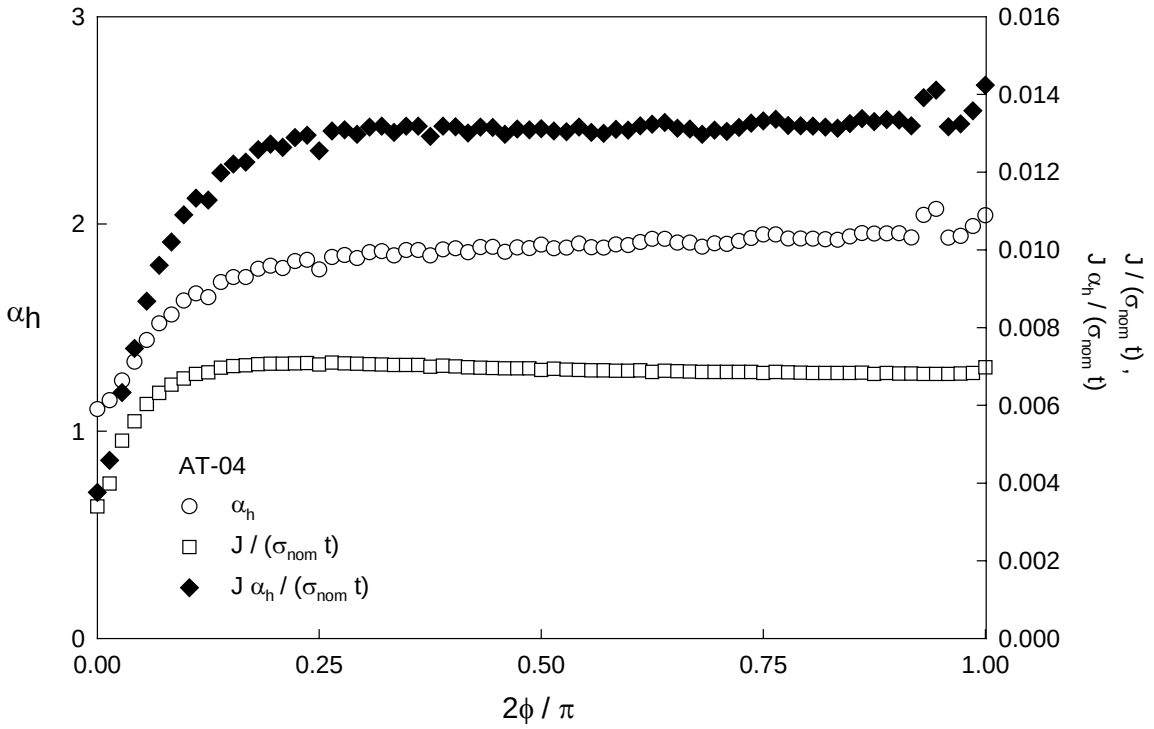

Figure B.1-2 AT-04 *J* and α_h Distribution (a = 3.20 mm, c = 4.44 mm, tension)

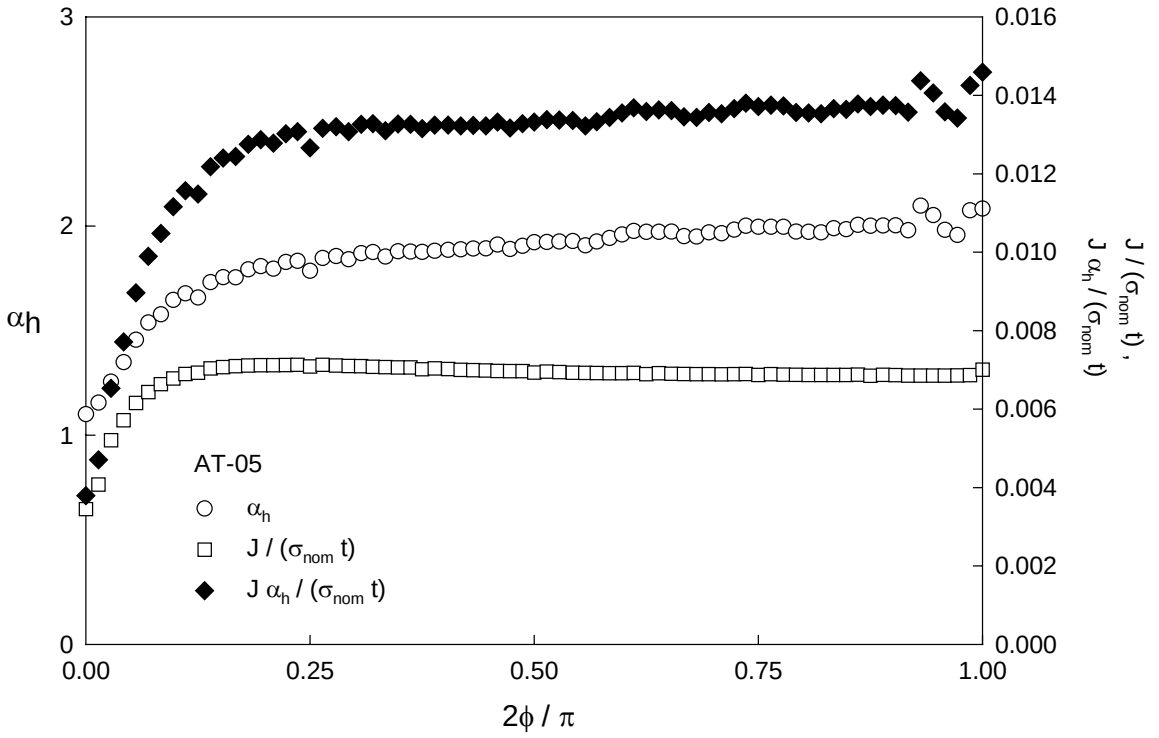

Figure B.1-3 AT-05 *J* and α_h Distribution (a = 3.33 mm, c = 4.75 mm, tension)

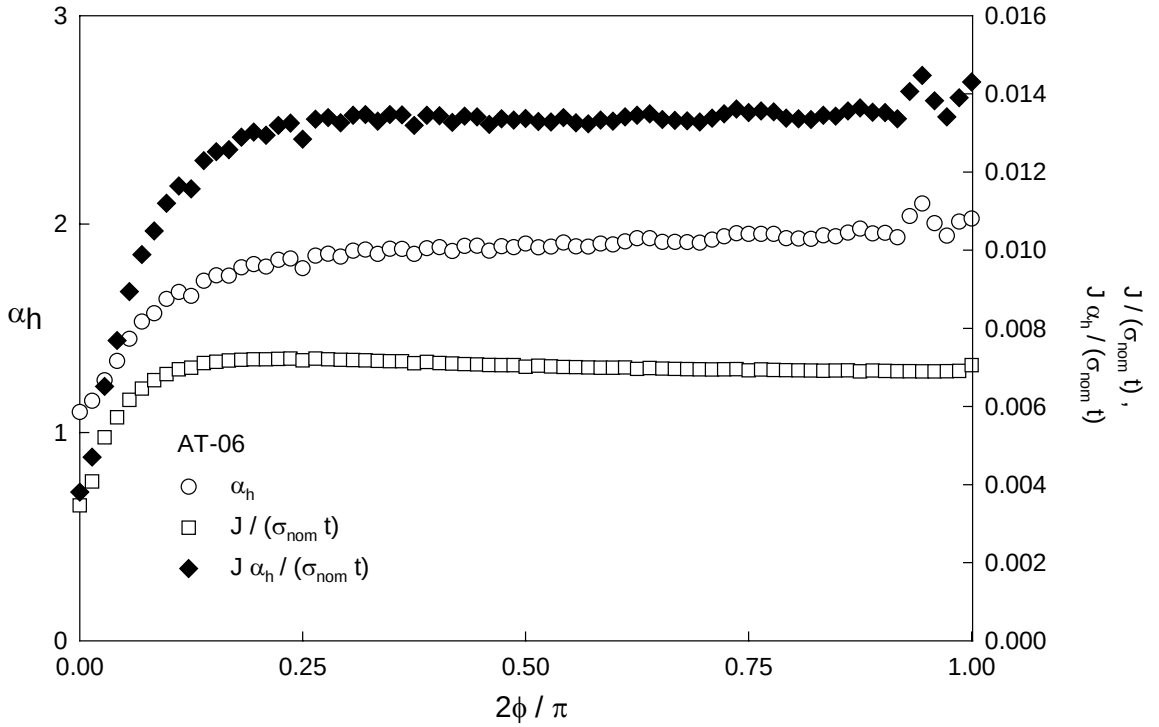

Figure B.1-4 AT-06 *J* and α_h Distribution (a = 3.27 mm, c = 4.56 mm, tension)

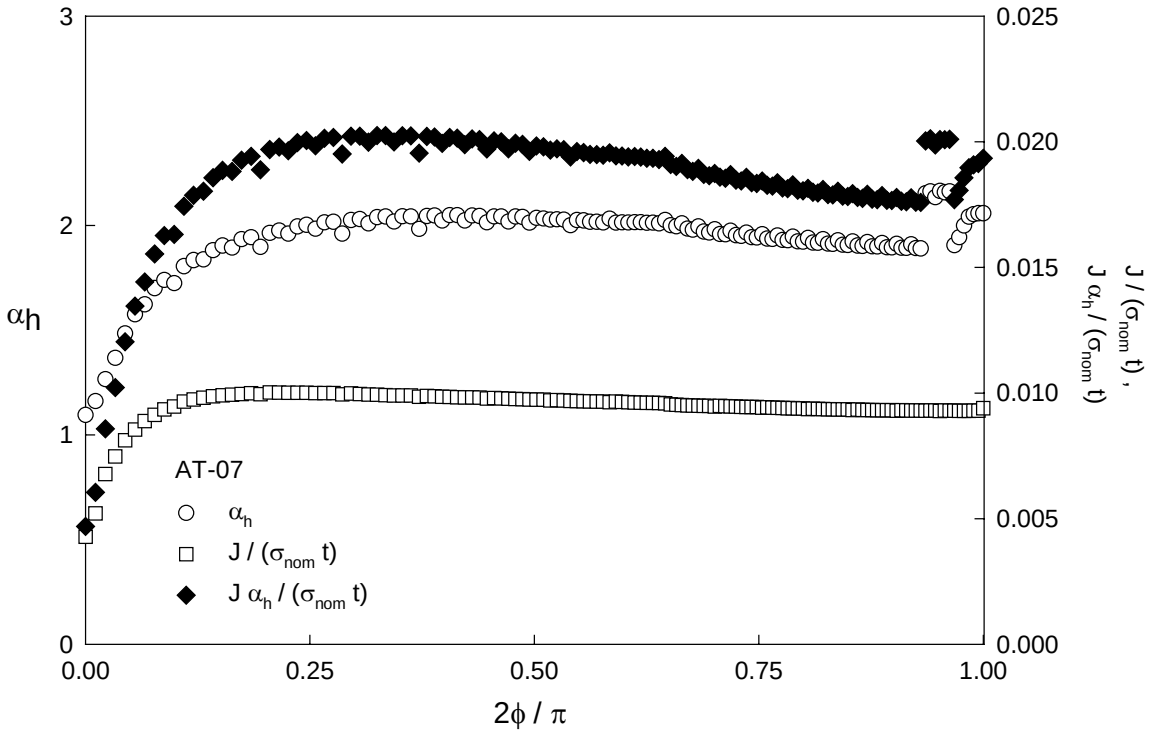

Figure B.1-5 AT-07 *J* and α_h Distribution (a = 4.13 mm, c = 6.78 mm, tension)

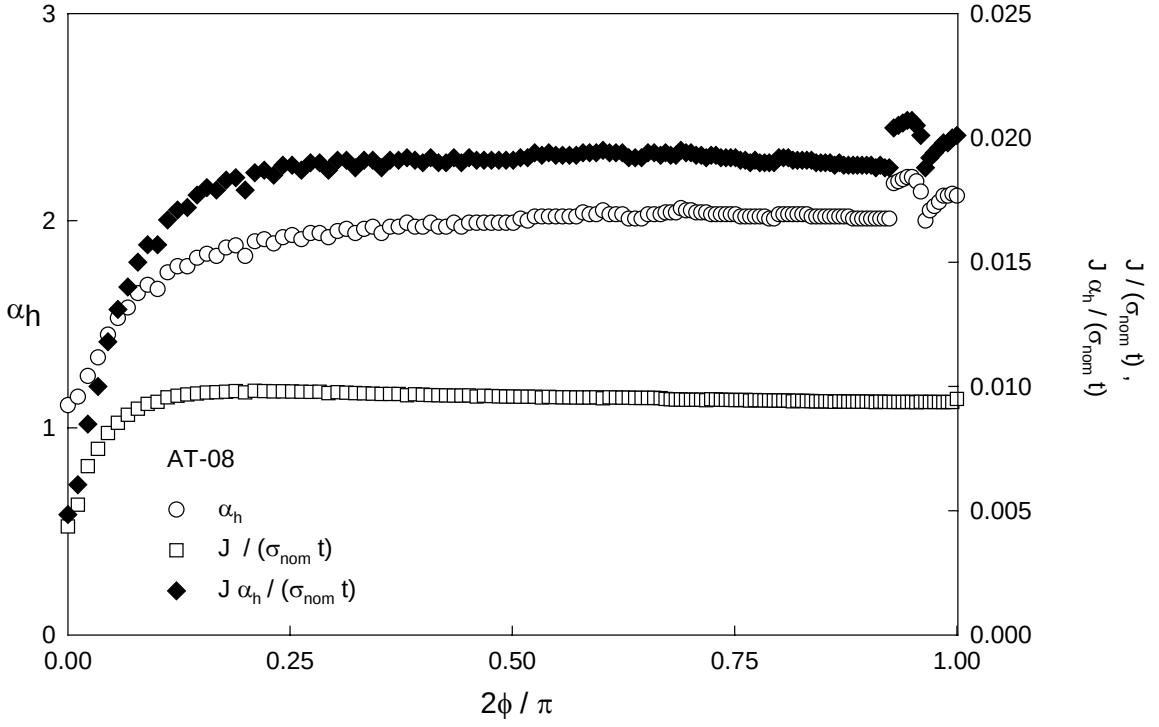

Figure B.1-6 AT-08 *J* and α_h Distribution (a = 4.27 mm, c = 6.97 mm, tension)

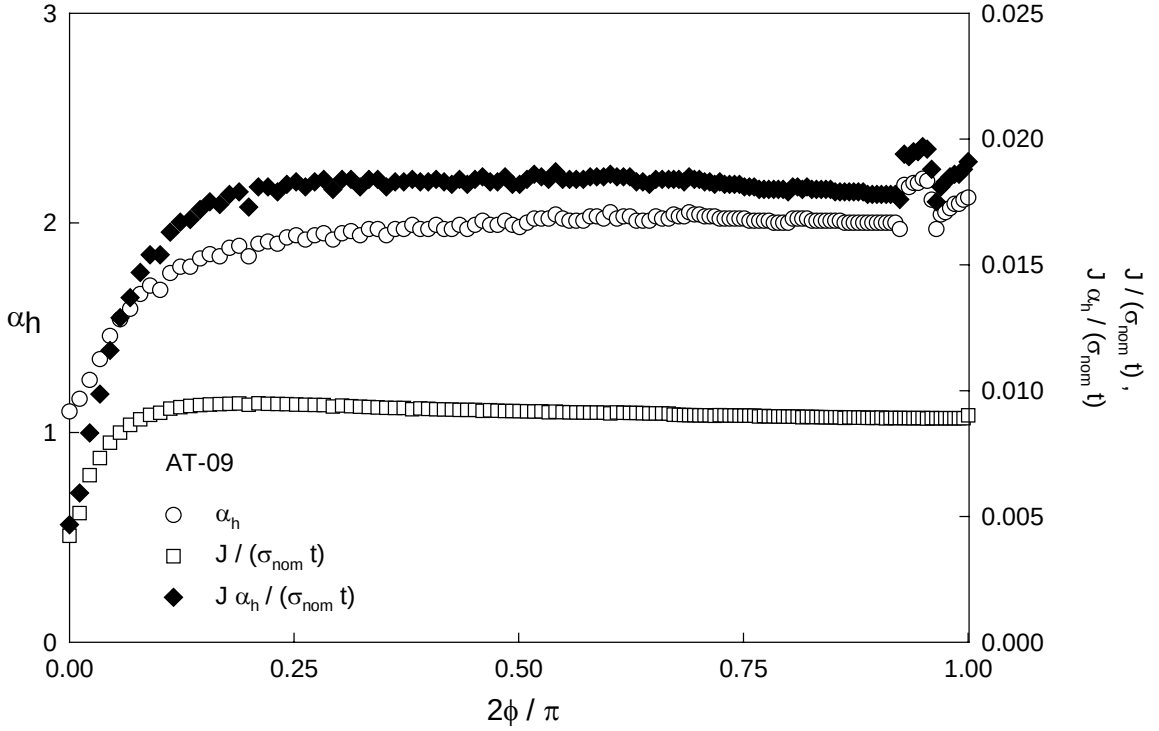

Figure B.1-7 AT-09 *J* and α_h Distribution (a = 4.16 mm, c = 6.63 mm, tension)

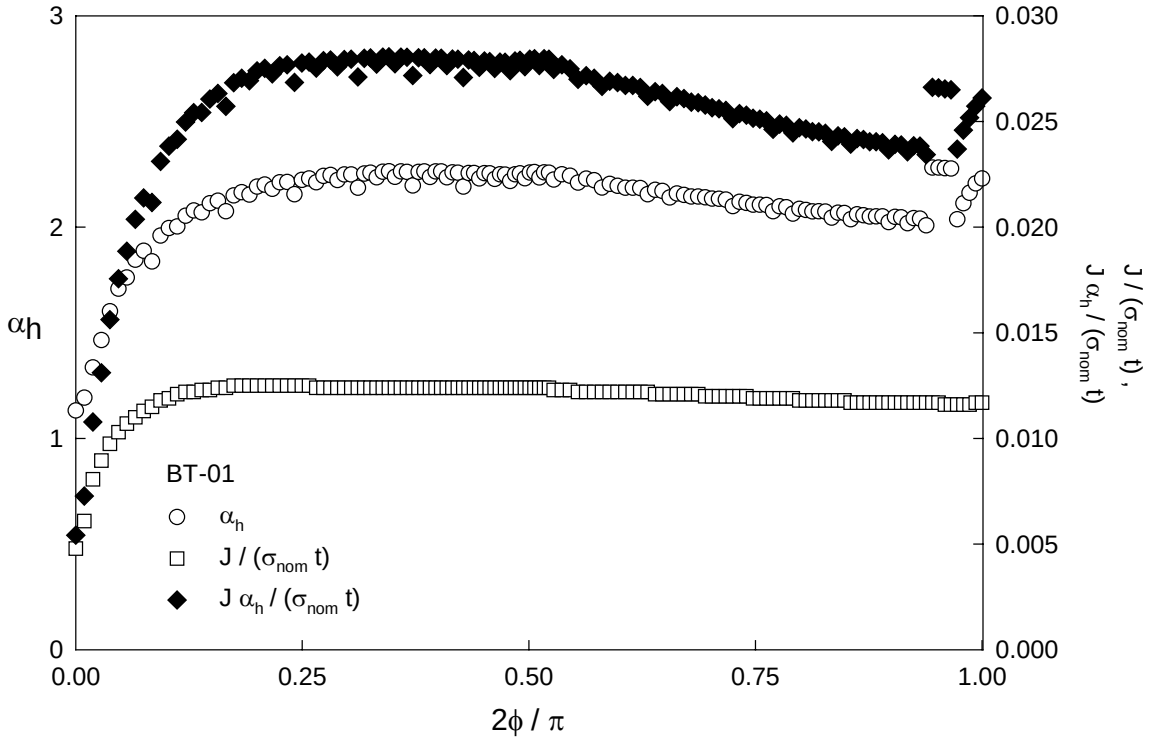

Figure B.1-8 BT-01 *J* and α_h Distribution (a = 4.61 mm, c = 9.80 mm, tension)

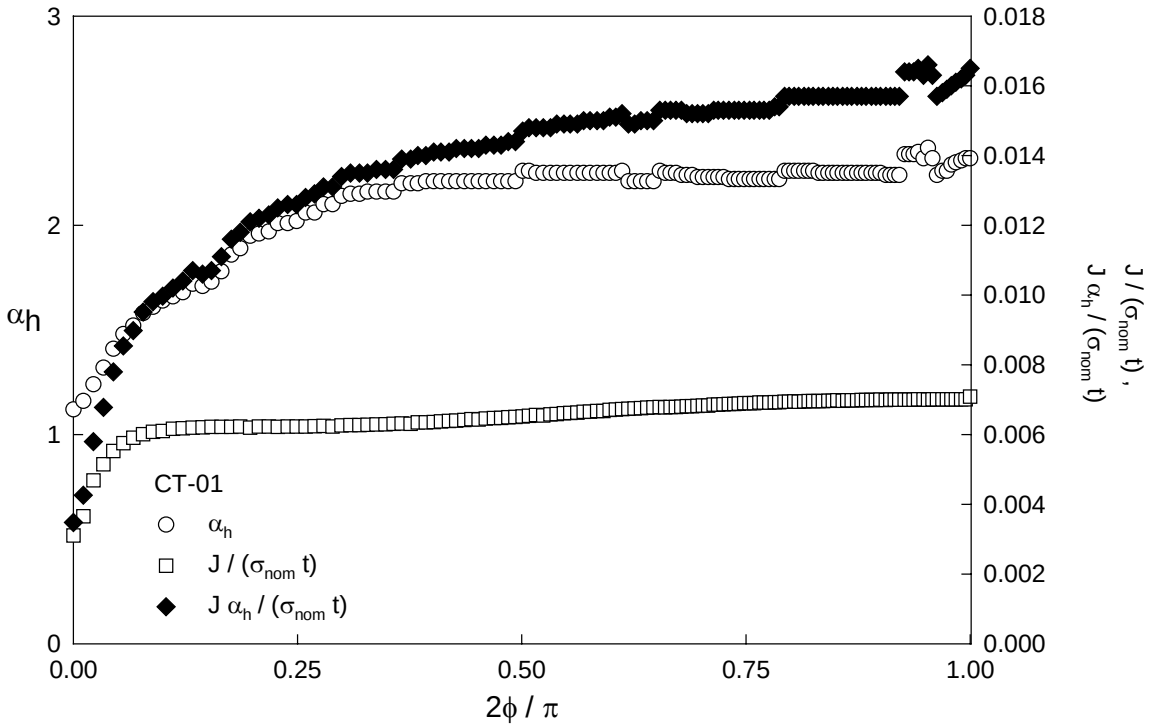

Figure B.1-9 CT-01 *J* and α_h Distribution (a = 3.49 mm, c = 6.44 mm, tension)

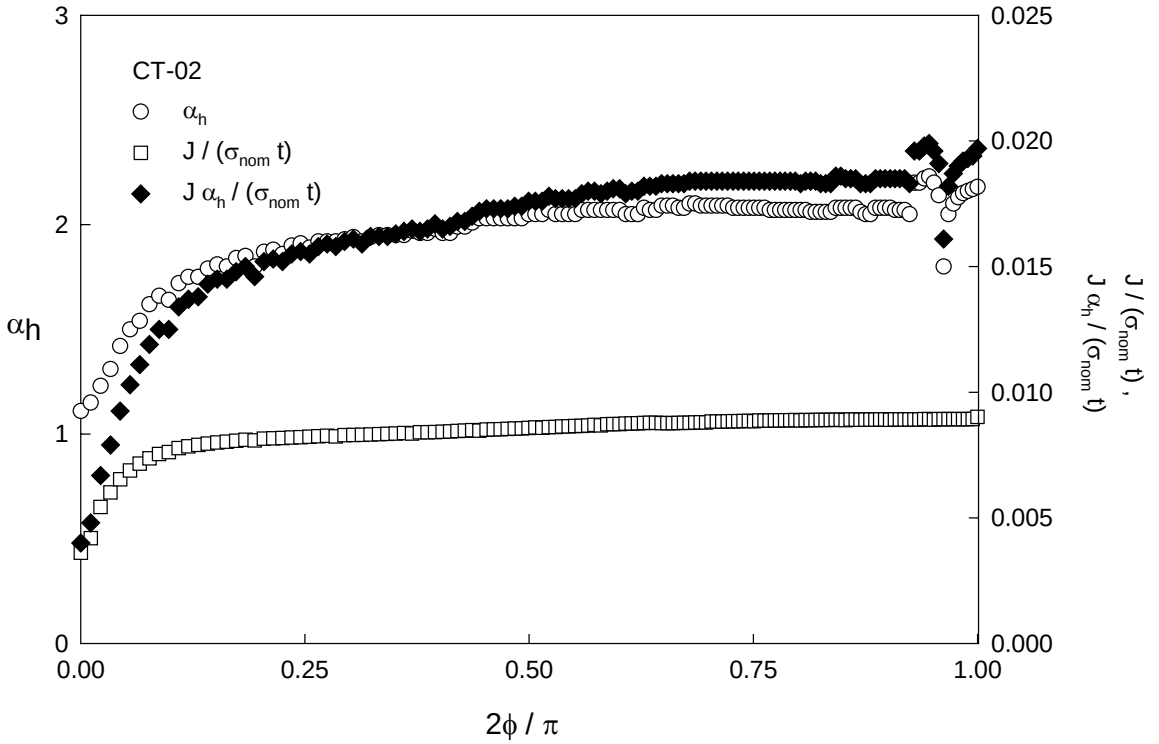

Figure B.1-10 CT-02 *J* and α_h Distribution (a = 3.51 mm, c = 6.65 mm, tension)

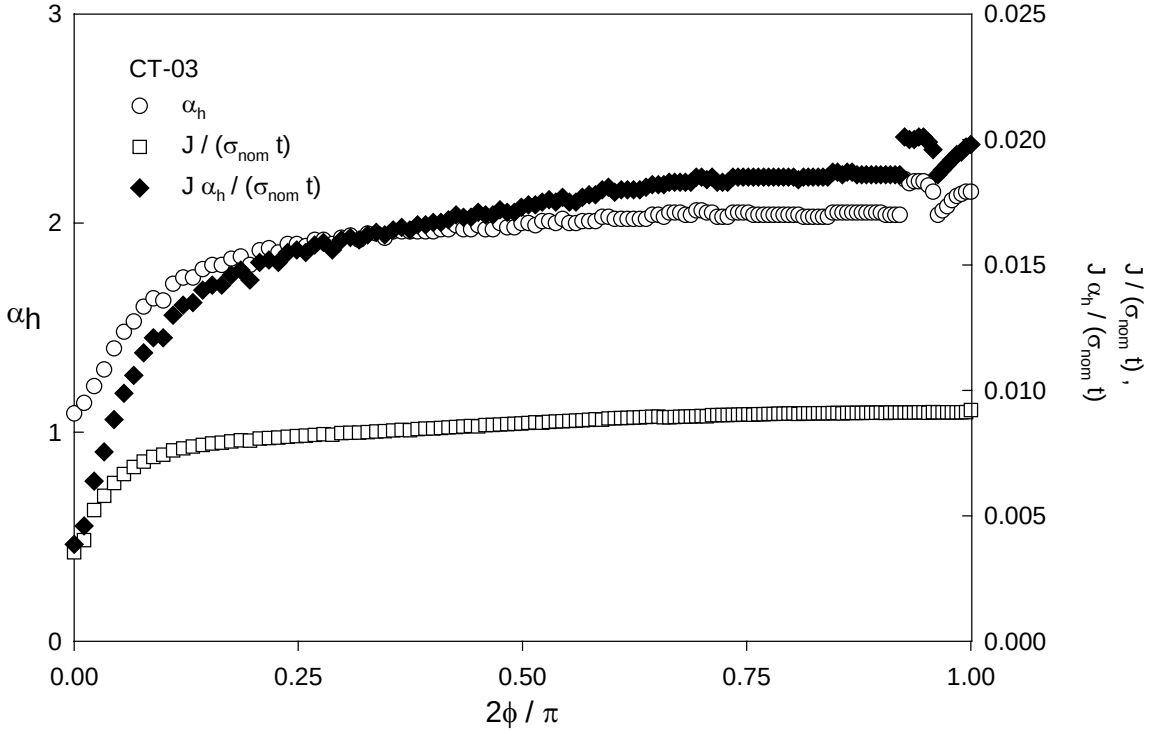

Figure B.1-11 CT-03 *J* and α_h Distribution (a = 3.38 mm, c = 6.56 mm, tension)

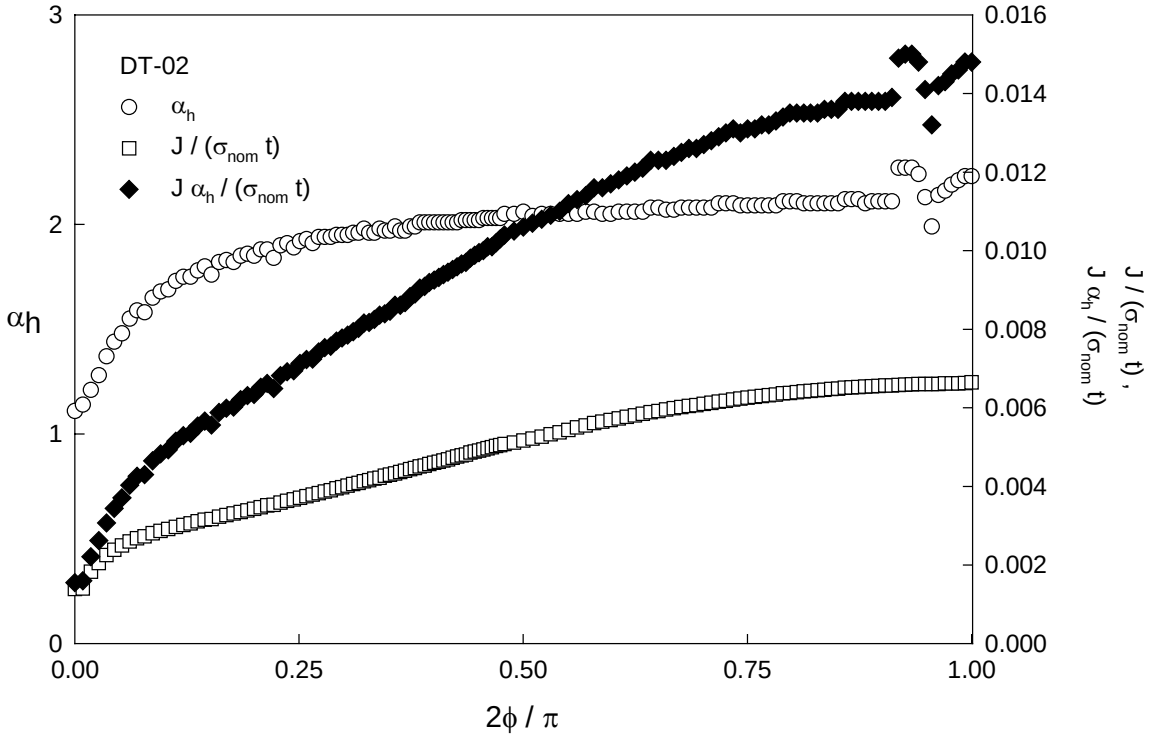

Figure B.1-12 DT-02 *J* and α_h Distribution (a = 1.73 mm, c = 6.42 mm, tension)

APPENDIX B.2

J-INTEGRAL AND α_h VARIATIONS

RESULTS – BENDING

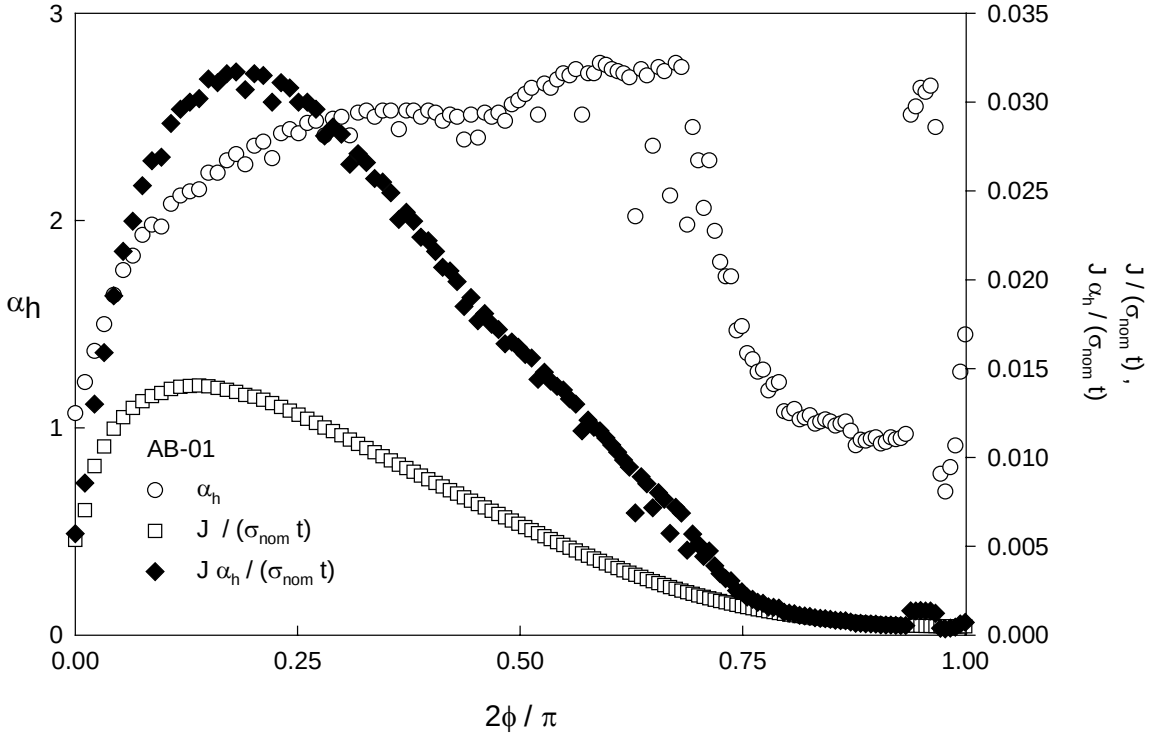

Figure B.2-1 AB-01 *J* and α_h Distribution (a = 4.356 mm, c = 7.076 mm, bending)

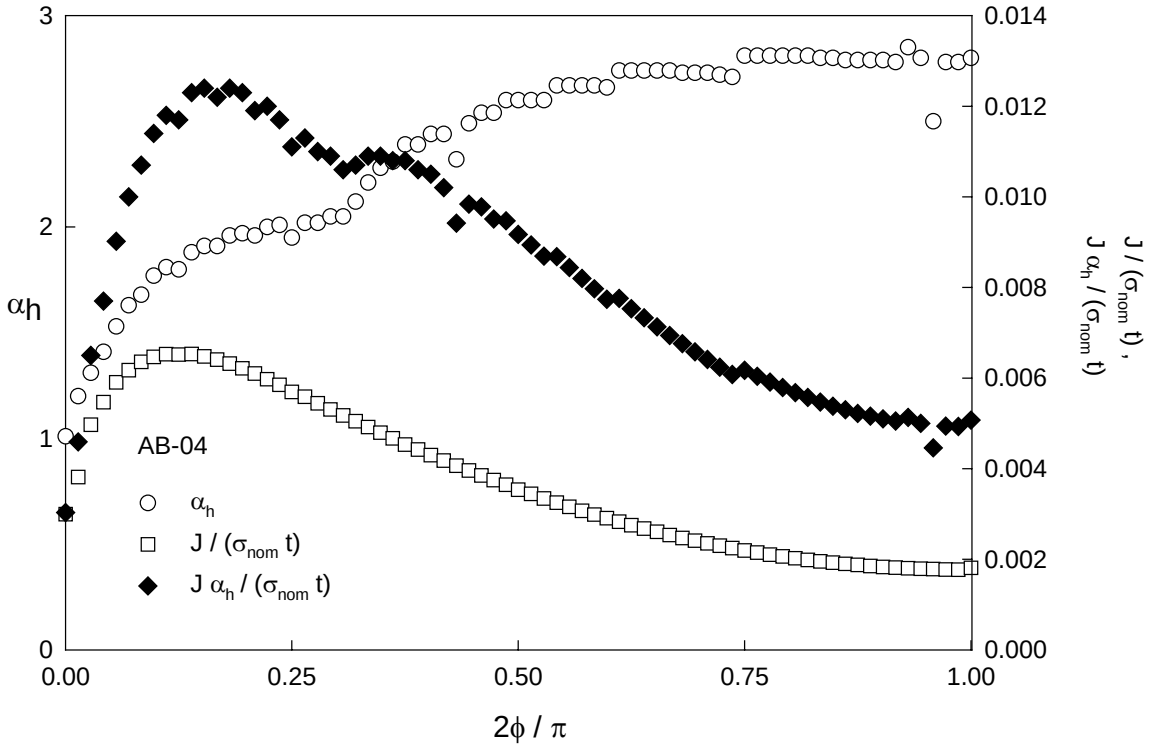

Figure B.2-1 AB-04 *J* and α_h Distribution (a = 3.185 mm, c = 4.543 mm, bending)

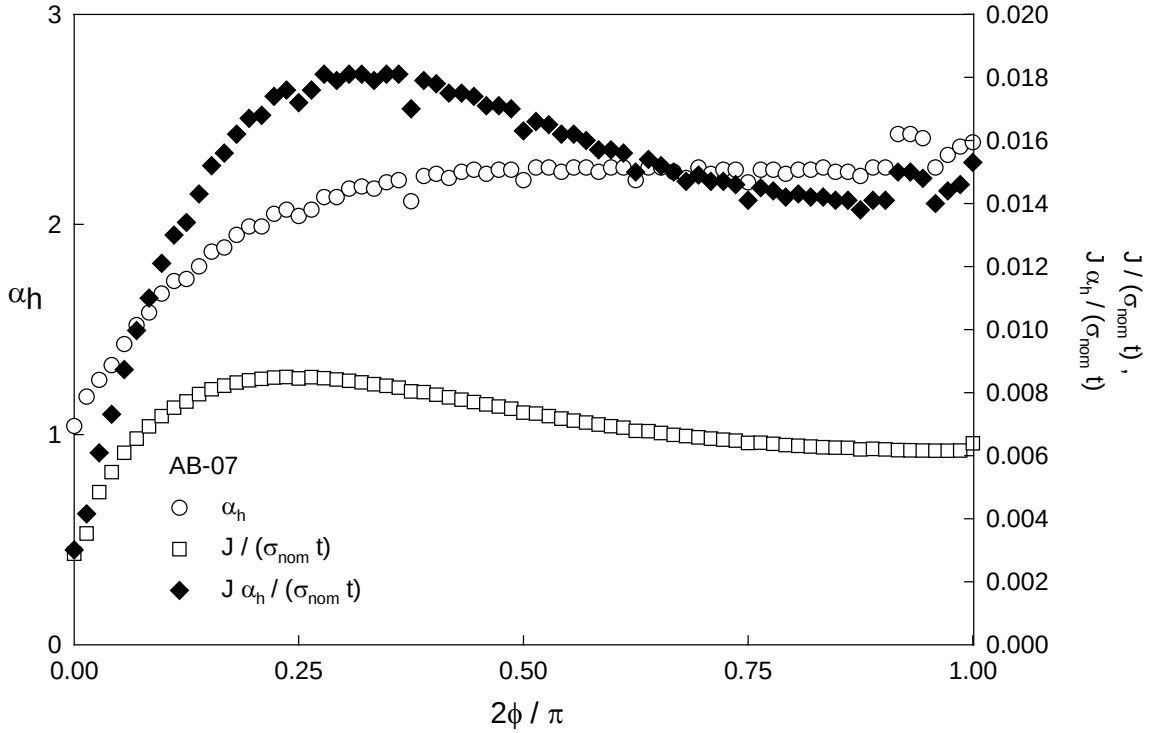

Figure B.2-3 AB-07 *J* and α_h Distribution (a = 1.516 mm, c = 1.822 mm, bending)

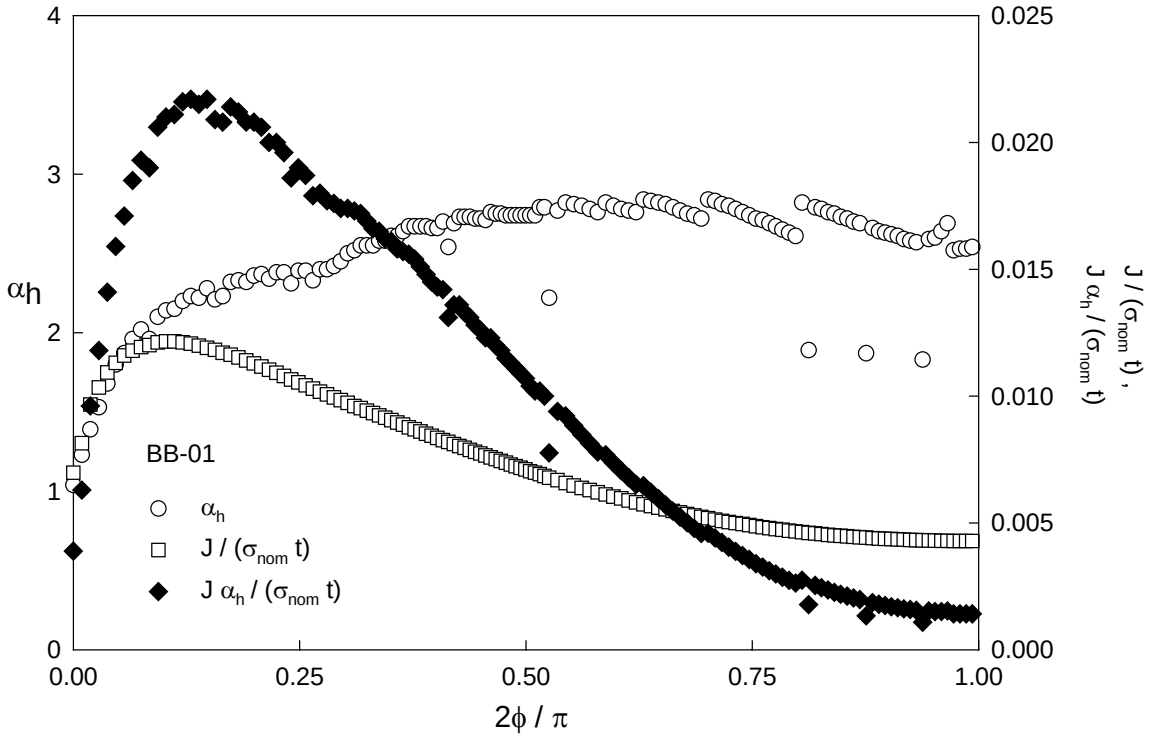

Figure B.2-4 BB-01 *J* and α_h Distribution (a = 4.62 mm, c = 9.86 mm, bending)

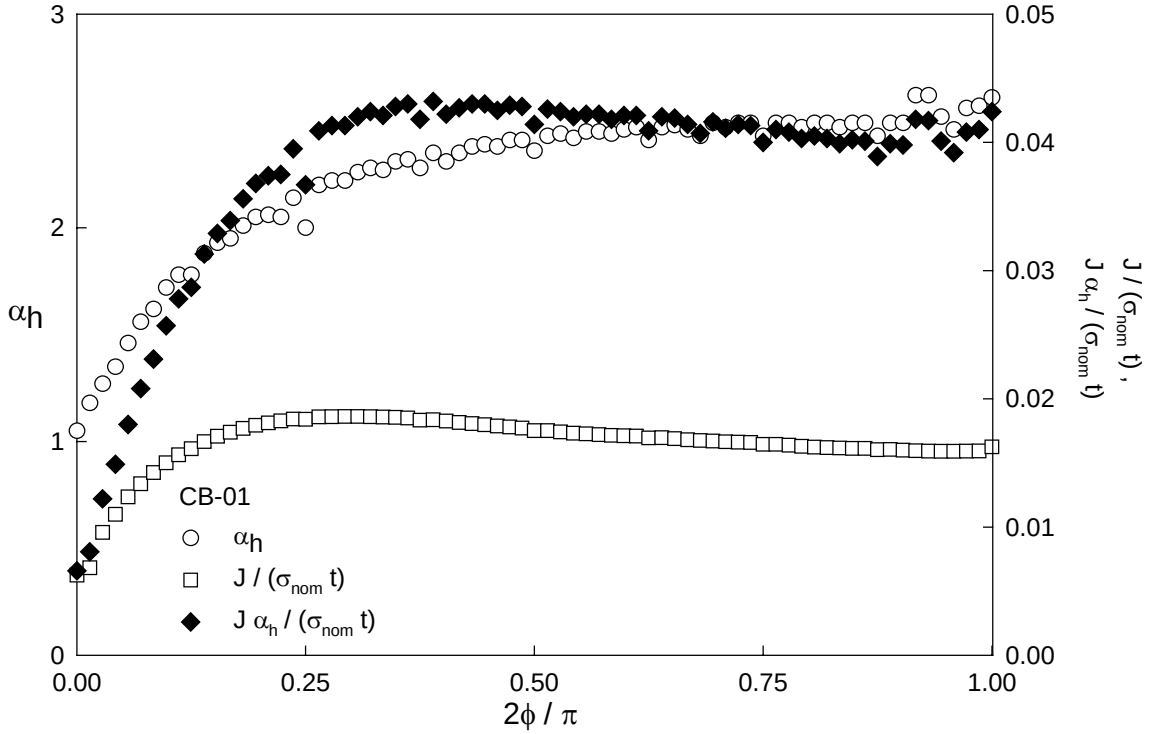

Figure B.2-5 CB-01 *J* and α_h Distribution (a = 1.712 mm, c = 2.69 mm, bending)

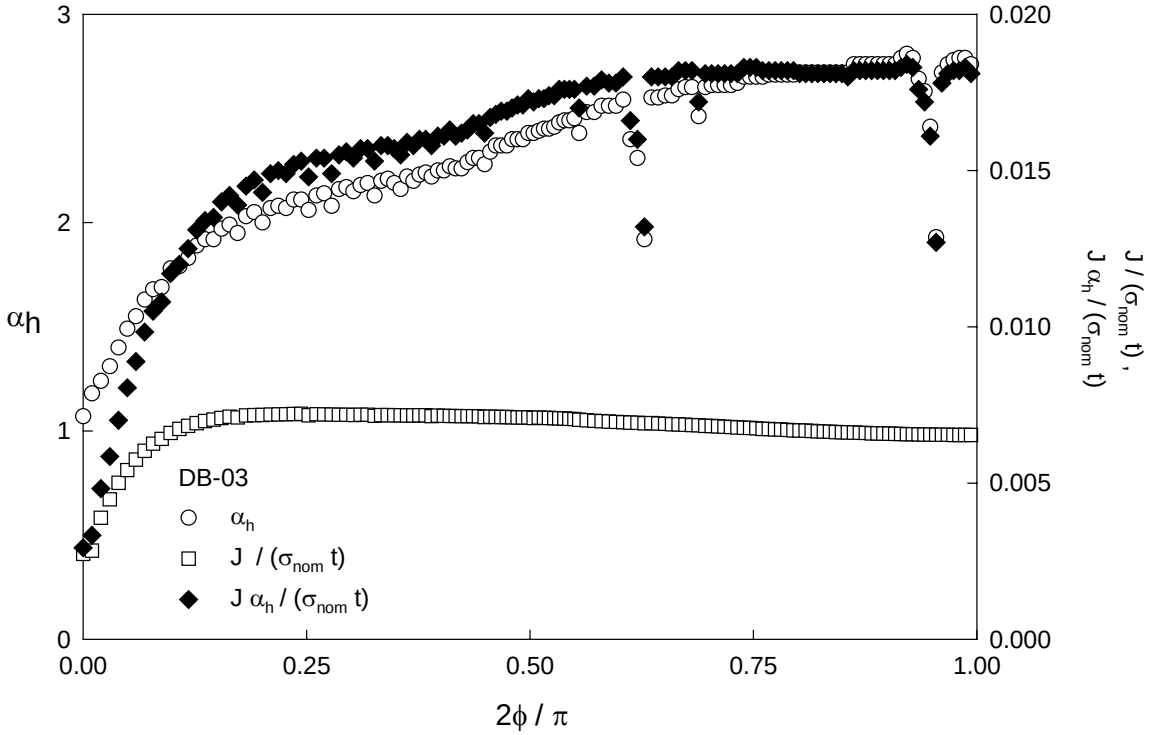

Figure B.2-6 DB-03 *J* and α_h Distribution (a = 2.314 mm, c = 6.487 mm, bending)

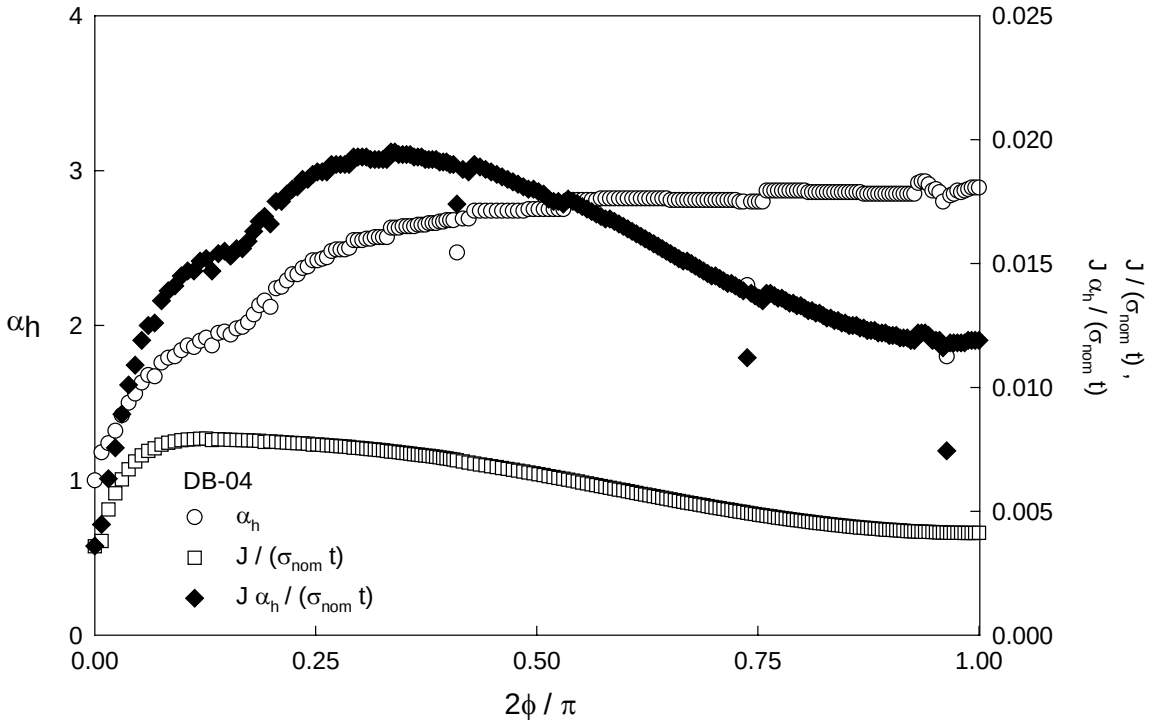

Figure B.2-7DB-04 *J* and α_h Distribution (a = 3.88 mm, c = 15.85 mm, bending)

APPENDIX C

CRACK EXTENSION CORRELATION TO $J\alpha_h$

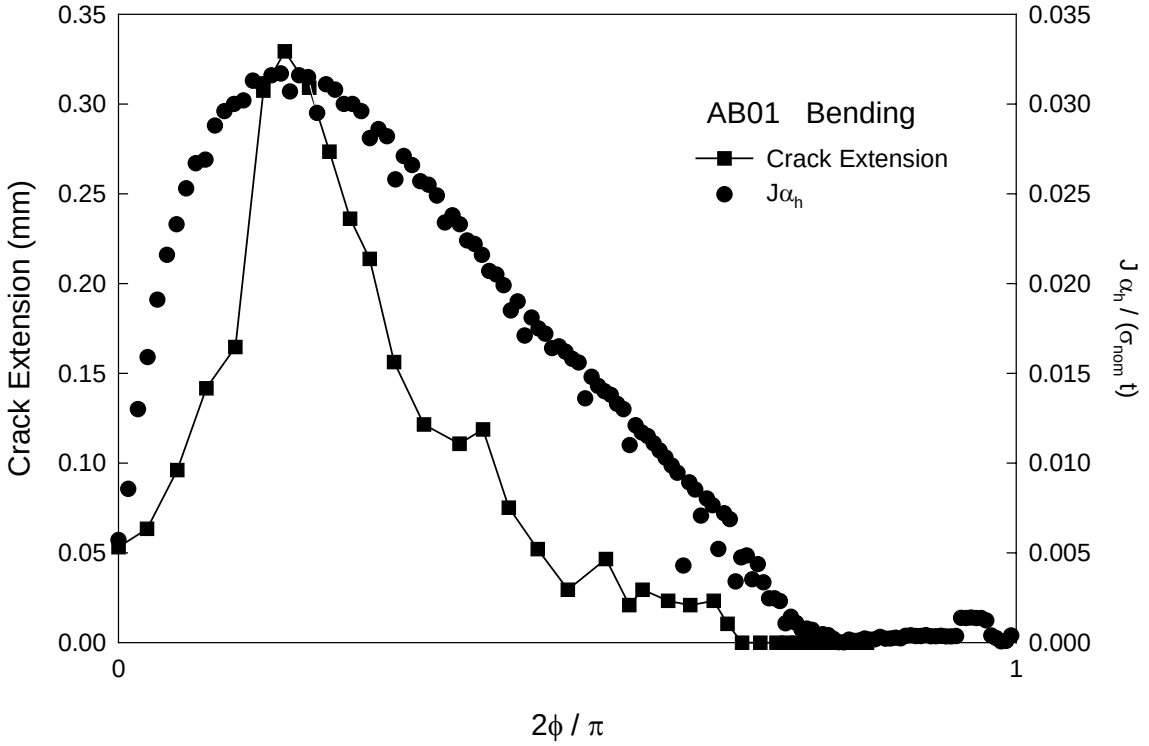

Figure C-1 AB-01 Crack Extension Correlated with $J\alpha_h$

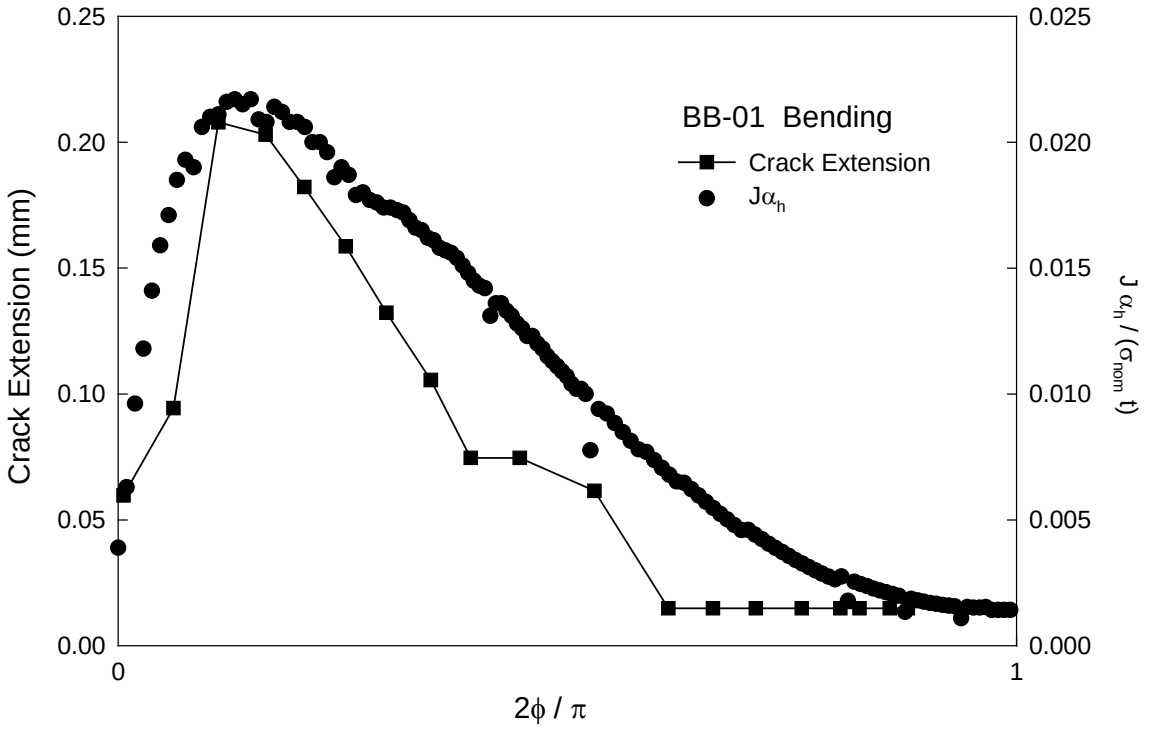

Figure C-2 BB-01 Crack Extension Correlated with $J\alpha_h$

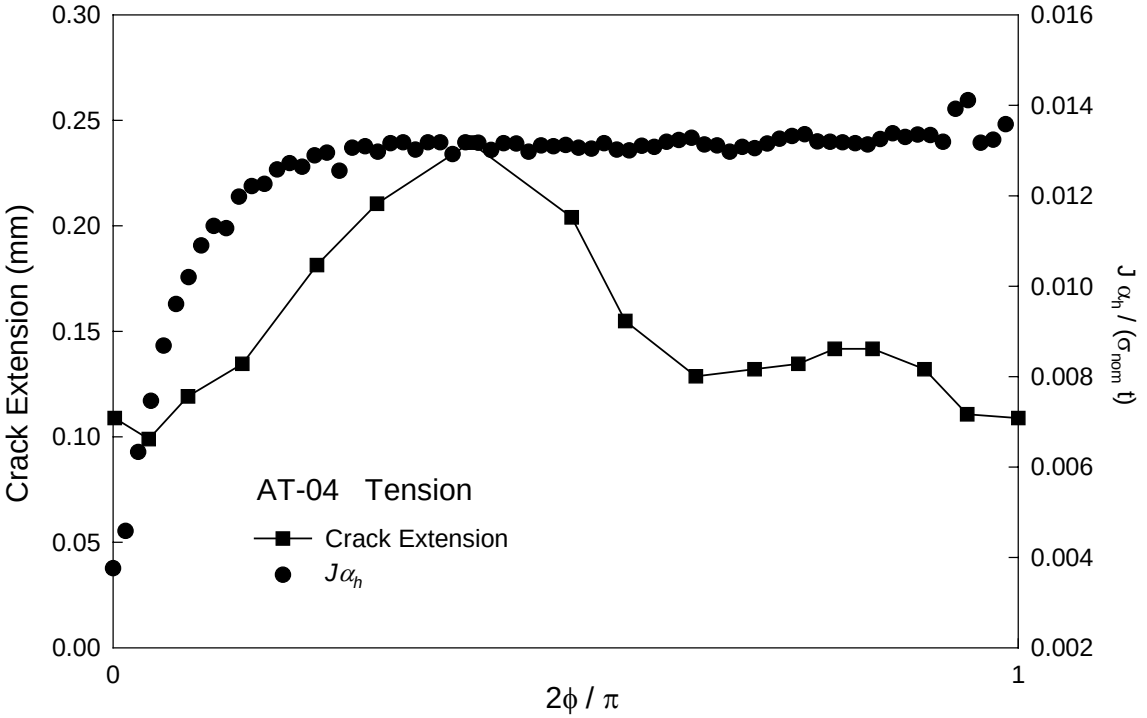

Figure C-3 AT-04 Crack Extension Correlated with $J\alpha_h$

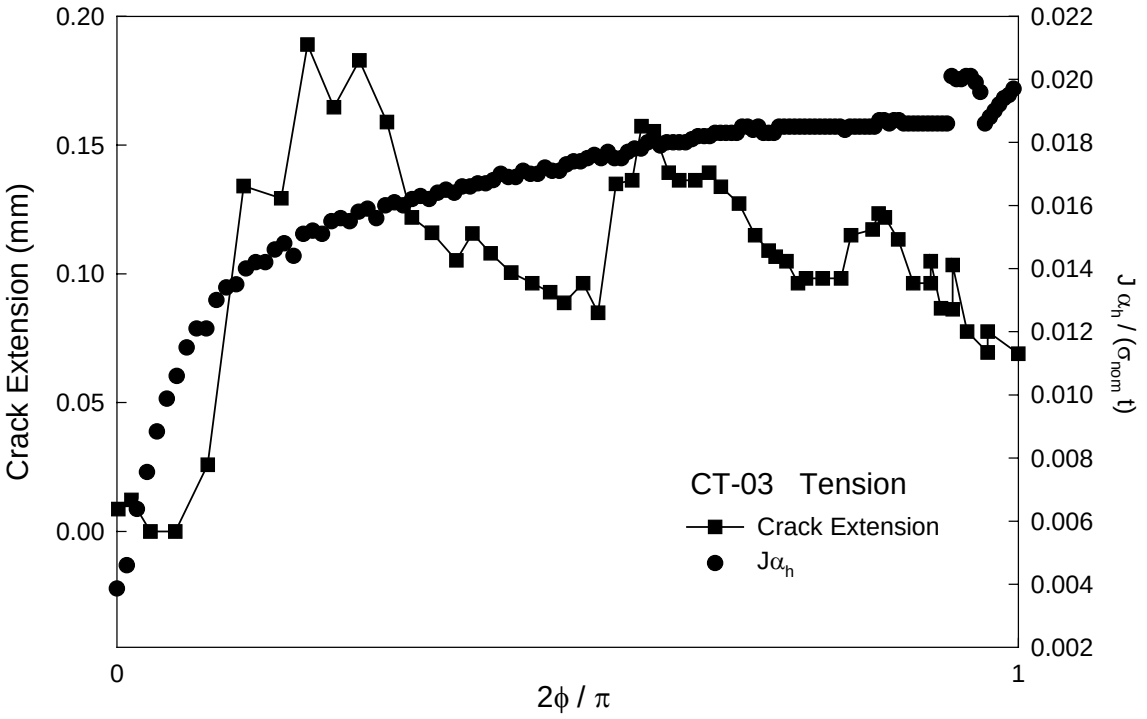

Figure C-4 CT-03 Crack Extension Correlated with $J\alpha_h$